Can Terahertz Provide High-Rate Reliable Low Latency Communications for Wireless VR?

Chaccour, Christina; Soorki, Mehdi Naderi; Saad, Walid; Bennis, Mehdi; Popovski, Petar

Published in:
IEEE Internet of Things Journal

DOI (link to publication from Publisher):
10.1109/JIOT.2022.3142674

Publication date:
2022

Document Version
Accepted author manuscript, peer reviewed version

This article has been accepted for publication in a future issue of this journal, but has not been fully edited. Content may change prior to final publication. Citation information: DOI 10.1109/JIOT.2022.3142674, IEEE Internet of Things Journal

Can Terahertz Provide High-Rate Reliable Low Latency Communications for Wireless VR?

Christina Chaccour*, Mehdi Naderi Soorki†, Walid Saad *, Mehdi Bennis‡, and Petar Popovski §
*Wireless@ VT, Bradly Department of Electrical and Computer Engineering, Virginia Tech, Blacksburg, VA USA,
†Faculty of Engineering, Shahid Chamran University of Ahvaz, Ahvaz, Iran,
‡Centre for Wireless Communications, University of Oulu, Finland,
§ Department of Electronic Systems, Aalborg University, Denmark.
Emails:{christinac, mehdin, walids}@vt.edu, mehdi.bennis@oulu.fi, petarp@es.aau.dk

***Abstract*—Wireless virtual reality (VR), a key 3GPP use case of emerging cellular systems, imposes new visual and haptic requirements directly linked to the quality-of-experience (QoE) of VR users. These QoE requirements can only be met by wireless connectivity that offers *high-rate and high-reliability low latency communications (HR2LLC)*, unlike the low rates commonly associated with ultra-reliable low latency communication. The high rates for VR over short distances can only be supported by an enormous bandwidth, available in the terahertz (THz) frequency bands. To explore the potential of THz for meeting HR2LLC requirements, a quantification of the risk for an unreliable VR performance is conducted through a novel and rigorous characterization of the tail of the end-to-end (E2E) delay. Then, a thorough analysis of the tail-value-at-risk (TVaR) is performed to concretely characterize the behavior of extreme wireless events crucial to the real-time VR experience. In particular, the probability distribution function of the THz transmission delay is derived and then used to infer the system reliability scenarios with guaranteed line-of-sight (LoS) as a function of THz network parameters. Numerical results show that abundant bandwidth and low molecular absorption are necessary to improve the reliability. However, their effect remains secondary compared to the availability of LoS, which significantly affects the THz HR2LLC performance. In particular, for scenarios with guaranteed LoS, a reliability of 99.999% (with an E2E delay threshold of 20 ms) for a bandwidth of $15\,\mathrm{GHz}$ along with data rates of $18.3\,\mathrm{Gbps}$ can be achieved by the THz network, compared to a reliability of 96% for twice the bandwidth, when blockages are considered.**

***Index Terms*—virtual reality (VR), cellular networks, reliability, performance analysis, terahertz (THz), risk.**

I. Introduction

Virtual reality (VR) applications have emerged as a key use case of wireless cellular as evidenced by recent industry, academic, and standardization efforts [1] and [2]. In order to integrate VR services over wireless cellular networks, it is imperative to equip the wireless network with the ability to meet the stringent quality-of-service (QoS) requirements of VR applications. On the one hand, it is important to ensure *reliable* low latency communications [2], i.e., the *instantaneous* end-to-end (E2E) delay for wireless VR must be very low to maintain a satisfactory user experience [3]. On the other hand, along with high-reliability, wireless VR services also require *high data rates* to deliver the 360° content to their users. Unlike the commonly considered low-rate ultra reliable low latency communications for the Internet of Things [4], VR requires *high-rate and high-reliability low latency communications (HR2LLC)* where high reliability and high rates are simultaneously needed for the transmission of large VR content packets [1]. Additionally, VR applications must immerse users in a seamless experience, and, thus, existing reliability definitions. e.g. [5], must be extended accordingly to encompass the unique timing requirements of VR. In particular, offering a high probability of successful transmission must be considered within a given (low) latency constraint.

This challenge can be addressed only through the use of abundant bandwidth, available at terahertz (THz) and millimeter wave (mmWave) frequencies [6]. In fact, the delayed deployment of the THz frequency band is due to the *THz gap* and the challenges accompanying semiconductor and optical transceivers at such frequencies [7]. Nonetheless, with the advent of plasmonic devices, and graphene-based designs, the aforementioned challenges were alleviated. As a result, novel tunable, high-speed, and energy-efficient THz transceivers started seeing light [8]–[10].

While early generations of VR services (up to full-view 12K video) can be delivered using mmWave systems, 5G remains limited by a maximum downlink data rate up to a few Gbps. Such a data rate can only fulfill the requirements of the *advanced* VR generation. Meanwhile, a new generation of VR services, dubbed *ultimate VR*, i.e., the new generation of VR that delivers higher video quality and a multi-sensory experience, will soon be deployed [11]. In ultimate VR, a data rate of $6.37 - 95.55\,\mathrm{Gbps}$ is needed (the range varies based on the compression technique used) [2], and that is clearly beyond the capabilities of today's mmWave 5G systems. Thus, this naturally motivates the migration towards THz frequency bands. In addition to the extremely high data rate needs, ultimate VR requires incorporating the five senses [12], which necessitates stringent *instantaneous low latency requirements*. Henceforth, in alignment with the current established 5G standard by 3GPP for 360-degree VR streaming services within

This research was supported by the National Science Foundation under Grant CNS-1836802.

Release-15 [13], this work envisions a need for a sustainable support of VR services by next-generation cellular systems. Moreover, beyond 5G systems support a migration towards higher frequency bands, namely sub-THz and THz bands, which require dealing with a high level of uncertainty. In particular, wireless systems at THz frequency bands are limited by a short communication range and a high susceptibility to molecular absorption, blockage and deep fades. This results in an on-off behavior of wireless links and leads us to the hypothesis that, if properly managed, THz can potentially offer HR2LLC: high rate concurrently with high reliability and low latency, to ensure an immersive VR experience. Investigation of this hypothesis is the subject of this work.

A. Prior Works

A number of recent works addressed the challenges of wireless VR [14]–[18]. The authors in [14] investigated the use of communication-constrained mobile edge computing (MEC) systems for wireless VR. In [15], the authors proposed a VR model using multi-attribute utility theory to capture the tracking and delay components of VR QoS. Recently, the problem of HR2LLC for VR networks was studied in [16]–[18]. For instance, in [16], the authors introduced an MEC-based mobile VR delivery framework that minimizes the average required rate. The work in [17] studied the challenge of concurrent support of visual and haptic perceptions over wireless networks. The authors in [18] proposed a joint proactive computing and mmWave resource allocation scheme for VR under latency and reliability constraints. However, the prior works in [15]–[18] only examine the average delays and data rates; thus reflecting limited information about the wireless VR systems analyzed. In contrast, to guarantee HR2LLC, *it is necessary to obtain the statistics of the delay in order to properly characterize the system's reliability.* Moreover, the works in [15]–[18] do not consider the more challenging reliability problem at high-frequency THz bands. Meanwhile, in [19] and [20], the authors investigate the ultra-reliability of wireless networks using a statistical approach. However, the works in [19] and [20] define reliability based on an outage event, while ignoring the E2E behavior of the system. Finally, the use of THz has recently attracted significant attention (e.g., see [6] and [21]–[25]) as an enabler of high data rate applications. However, these prior works in [6] and [21]–[25] focus primarily on the physical layer, and they do not address HR2LLC challenges for wireless VR. Meanwhile, in [26], we have conducted a performance analysis assessing how and when a THz network can meet the reliability, low latency and high data rate requirement. However, our work in [26] does not take into account realistic THz dynamic network conditions as it ignores the effect of self and dynamic blockages and focuses on idealized settings. Furthermore, given that the real-time dynamic nature of THz wireless systems complicates the tractability of the performance analysis, novel analytical frameworks must be proposed to formulate the performance limits of the system. Clearly, there is a lack in existing works that study the potential of THz frequencies to deliver HR2LLC VR services.

B. Contributions

This work provides a comprehensive analysis of delay, reliability, and rate, for a wireless THz network that serves VR users. The specific contributions are:

- To examine the *instantaneous* reliability of a wireless VR system, we derive the tail distribution of the E2E delay, including queuing and transmission delays over THz links, via its moments. This allows us to characterize the performance of a wireless VR system at extreme events while shedding light on THz's potential despite its short communication range and its high susceptibility to blockages and molecular absorption. To scrutinize the risk of an unreliable VR user experience at THz, we derive the tail-value-at-risk (TVaR) of the E2E delay based on rigorous tools from extreme value theory (EVT) and economics [27], [28]. Our analysis is unique with respect to its novel analytical framework (instantaneous and tail-risk approach) and its application (wireless VR operating at THz frequencies).
- Our analysis shows that the probability of line-of-sight (LoS) at THz frequencies, which is influenced by the density of VR users and their mobility, plays a primary role in characterizing the moments of the E2E delay. These results allow to characterize the tail distribution of the E2E delay using the instantaneous VR content requests, channel, and blockage parameters. Important insights are offered by the expected worst-case E2E delay, and the confidence level associated with the reliability.
- The asymptotic analysis of reliability is tailored to the unique THz network parameters. It characterizes the E2E delay distribution by finding the cumulative distribution function (CDF) of the E2E delay after deriving the probability distribution function (PDF) of the transmission delay in a dense THz network.

To our best knowledge, *this is the first work that performance a tail and risk analysis on the reliability and latency achieved by VR services over a THz cellular network.*

C. Main Findings

Following these contributions, we answered the question of *"Can THz provide high-rate reliable, low latency communications for wireless VR?"* as follows:

- For wireless VR services over THz networks, the characterization through quantities related to average delay lead to overly optimistic performance prediction at THz. Instead, tail delays reflect the performance during extreme events, such as a deep fade or a blockage. Analysis of extreme events is fundamental, as the occurrence of any such event during a VR session will lead to a disruption of the quality-of-experience (QoE). For example, our results show that, during a typical VR session THz the tail of E2E delay can range from $30\,\mathrm{ms}$ to $90\,\mathrm{ms}$ leading to an unreliable VR experience, even when the average delay is $20\,\mathrm{ms}$. Hence, achieving HR2LLC requires new

This article has been accepted for publication in a future issue of this journal, but has not been fully edited. Content may change prior to final publication. Citation information: DOI 10.1109/JIOT.2022.3142674, IEEE Internet of Things Journal

mechanisms that can guarantee LoS link and alleviate the harsh propagation conditions at THz. For example, such is the intelligent environment based on large multiple-input and multiple-output (MIMO) arrays [21] and [29].

- From our results, we observe that increasing the bandwidth and reducing the THz molecular absorption coefficient can reduce the risk of worst-case extreme events, but are not sufficient to sustain a reliable experience. Moreover, guaranteeing a TVaR with confidence levels (i.e. the reliability during extreme events) above $90\,\%$ is only possible at tail delays of $100\,\mathrm{ms}$, even at a significant bandwidth of $30\,\mathrm{GHz}$.
- One of the most fundamental challenges to THz's reliability is the availability of LoS component. Overcoming this challenge, ensures that THz can provide HR2LLC via network densification and significant bandwidths. In particular, our results show that, if one can ensure that the THz network can continuously operate at LoS, a reliability of 99.999% (with an E2E delay threshold of 20 ms) is achievable along with data rates of $18.3\,\mathrm{Gbps}$, thus, delivering promising rates to support ultimate VR's needs.

The rest of the paper is organized as follows. Section II introduces the system model. Sections III and IV, respectively, present the reliability analysis and asymptotic analysis of reliability. Section V presents the simulation results and conclusions are drawn in in Section VI.

II. System Model

Consider the downlink of a small cell network servicing a set $\mathcal{V}$ of V wireless VR users via a set of small base stations (SBSs) operating at THz frequencies and densely distributed in a confined indoor area according to an isotropic homogeneous Matern hardcore point process (MHCPP) with intensity η and a minimum distance ϵ [30]. This process is a special thinning of the Poisson point process (PPP) in which the nodes are forbidden to be closer than a minimum distance ϵ, as in practice the distance between adjacent SBSs cannot be arbitrarily small. Hence, this process can adequately capture the distribution of VR SBSs in a confined area. In our network, SBSs can also perform MEC functions for VR purposes and the VR users are associated to the SBS with highest signal-to-interference-plus-noise-ratio (SINR).

A. Wireless Model

We consider an arbitrary VR user in $\mathcal{V}$ located at a constant distance r_0 from its serving SBS. The chosen VR user and its serving SBS are referred to as *tagged* receiver and transmitter respectively. The interference surrounding this VR user stems from a set $\mathcal{M}$ of M non-negligibly interfering SBSs that are located within a radius of Ω around this user. Henceforth, SBSs that are at a distance $r \geq \Omega$ add no interference on the link between the VR user and its associated SBS, Ω refers to the region of non negligible interference of the network. It is important to note that interference occurs because we consider a highly dense THz network whose SBSs are located at very close proximity [31]. Indeed, if there are models in mmWave that consider interference after certain density of SBSs, then there must be a higher density of THz SBSs for which the interference becomes relevant. Moreover, in such a dense environment, THz bands require a very narrow pencil beamforming (even narrower than mmWave). Such beamforming architectures face major practical challenges given that they require a high available SINR link and a narrow beamsteering angle, while providing localization and tracking of the user equipment (UE) [32]. This also leads to higher susceptibility towards mobility, and does not completely solve the interference problem, given the difficulty to perform beam re-alignment in a short time [33].

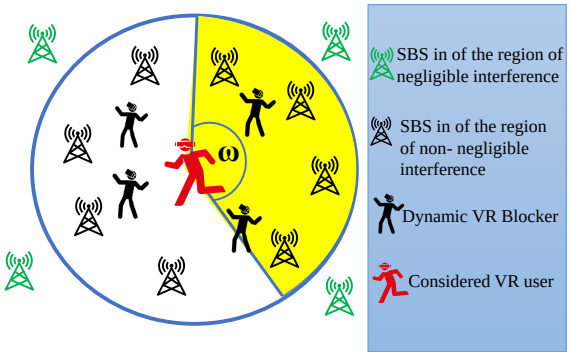

Figure 1: Illustrative example of the blockage and interference model.

Another key challenge facing THz communications in such a dense network is the inability to penetrate solid objects. In fact, the electromagnetic properties of THz are different than conventional bands, i.e., their penetration losses are higher whereas their reflection coefficients are reduced[1] [34]. Subsequently, the susceptibility of THz to blockage jeopardizes its reliability, thus, highlighting the importance of studying the probability of blockage, that further provides insights about the tunable parameters needed to guarantee a LoS link between the SBS and the VR user. We consider two types of indoor blockages: self-blockage and dynamic blockage. *Self-blockage* arises when a user blocks a fraction of SBSs by its own body. Each user makes an angle ω with the blocked SBSs. ω determines the orientation of the user and is assumed to be uniformly distributed in $[0,2\pi]$, as shown in Fig. 1. The uniform probability here captures the free range of motion of mobile VR users in all directions. Real-world experiments in [35] show that the azimuth angle follows closely a uniform distribution along $[-\pi,\pi]$, thus, confirming our choice. The self-blockage zone is defined as the sector of a disc of radius B having an angle ω. Without loss of generality, hereinafter, we assume that $B = \Omega$, i.e., the blockage disc and the region of non-negligible interference coincide, and, thus, we will use Ω to refer to this region. This assumption is justified

[1]This behavior is similar to mmWave bands but is more pronounced for THz. For instance, while the molecular absorption effect might be negligible for mmWave bands, it is more significant at THz and it must be accounted for.

This article has been accepted for publication in a future issue of this journal, but has not been fully edited. Content may change prior to final publication. Citation information: DOI 10.1109/JIOT.2022.3142674, IEEE Internet of Things Journal

Table I: List of our main notations.

Notation	Description	Notation	Description
V	Wireless VR users	ϵ	Minimum MHCPP distance
η	Intensity of SBS according to MHCPP	η_p	Equivalent Poisson intensity of SBSs
r	Distance between SBS and VR user	M	Number of interfering SBSs
Ω	Radius of non-negligible interference	B	Radius of blockage region
ω	Angle of self-blockage	Q	Number of SBSs susceptible to blockage
ι_B	Intensity of dynamic blockers	v_B	Velocity of dynamic blockers
κ_B	Arrival of blockers to blockage queue	ν	Departure of blockers from blockage region
Λ	LoS event	N	Noise
L	VR image size	W	Bandwidth
p_0	Tagged transmission power	p_i	Interfering transmission power
T	Temperature	$K(f)$	Overall absorption coefficient of the medium
f	Frequency	C_L	LoS Path rate
α	Transmission delay	I	Interference
μ_I	Mean of the interference	σ_I^2	Variance of the interference
T_1	Total waiting time in Q_1	T_2	Total waiting time in Q_2
μ_1	Service rate at Q_1	λ_1	Arrival rate at Q_1
μ_2	Service rate at Q_2	λ_2	Arrival rate at Q_2
ϑ	Variance	α_C	Confidence level
VaR	Value-at-risk	χ	Tail-value-at-risk

given that interferers and blockages are only non-negligible within a specific radius around a given VR user. Thus, this region draws the boundaries of the THz link range around a given user. An SBS is thus considered to be *self-blocked* if it lies in the self-blockage region of the considered VR user. Hence, the probability of self-blockage will be [36]: $P(B_s) = \frac{\omega}{2\pi}$, where B_s is a random variable that captures self-blockage event. *Dynamic blockage* captures the event in which the LoS signal between the considered VR user and its serving SBS is interrupted by other users. The users contributing to dynamic blockage are moving in a blockage area of radius Ω within which a set $\mathcal{Q}$ of q SBSs are susceptible to blockage. The VR users in this region are *dynamic blockers* that move in a random direction with velocity v_B, and they are distributed according to a homogeneous PPP with density ι_B. Thus, the overall dynamic blockage process can be modeled as an M/M/∞ queuing system[2], as explained in [36]. The first M stands for a Poisson arrival process of blockers with a rate of κ_{Bi} blockers/sec, and the second M stands for a blockage duration that is assumed to be exponentially distributed with parameter ν blockers/sec. For tractability, we use the approach from [36] to model the dynamic blockage and further approximate the MHCPP by an equivalent PPP of intensity η_P. This is justified by the fact that our dense network will naturally have small distances between SBSs. Beyond this blockage modeling, we keep the deployment according to an MHCPP rather than a filtered PPP. A simultaneous blockage event by two or more dynamic blockers for the same LoS link is a negligible (null) event because of the short range of THz links and the low likelihood of two users simultaneously disrupting a link of a few meters. Let $\boldsymbol{r} \triangleq (r_i)_{i=0,1,\cdots,q}$ be a row vector, where r_0 is the distance between the VR user and its SBS, and r_i is the distance between the VR user and the blocked SBS $i \in \mathcal{Q}$. The SBS distances to the VR user are independently and identically distributed (i.i.d.) with distribution $f(r_i|q) = \frac{2r_i}{\Omega^2}$. Hence, the probability of dynamic blockage is [36]: $P(B_d|r_i, q) = \frac{\kappa_{Bi}}{\kappa_{Bi}+\nu}$, and the probability of simultaneous blockage of all LoS links is given by:

$$P(B|q, \boldsymbol{r_i}) = \prod_{i=1}^{q} P(B_i|q, \boldsymbol{r_i})$$
$$= \prod_{i=1}^{q} [1 - (1 - P(B_s))(1 - P(B_d))] = \prod_{i=1}^{q} (1 - \varkappa \frac{1}{1 + \frac{\Delta}{\nu} r_i}). \quad (1)$$

where $\varkappa$ is the probability that a random SBS is not self-blocked and $\Delta = \frac{2}{\pi} \iota_B v_B \frac{(h_B - h_R)}{(h_T - h_R)}$ where h_B, h_R, and h_T are, respectively, the height of the dynamic blocker, the height of the considered VR user, and the height of the SBS. Also, Δ is related to the blockage rate by the following $\Delta = \frac{\kappa_{Bi}}{r_i}$. The channel and data rates of THz links are modeled next.

B. Data Rate Formulation

As shown in [31], the THz signal propagation is mainly affected by molecular absorption[3], which results in molecular absorption loss and molecular absorption noise. At THz, the gap between the LoS and non-line-of-sight (NLoS) links is very significant and more drastic than at mmWave frequencies. Given that the distance between a VR user and its respective SBS is short in our dense network, we consider only the LoS

[2]While an ideal model would follow an M/G/∞ queue as an alternating renewal process with exponentially distributed periods of blocked and unblocked intervals, similar to [37], such a model applied to our setting lacks tractability. Hence, for mathematical simplicity, and as done in [36], the dynamic blocker arrival process is relaxed to an M/M/∞.

[3]The molecular absorption can be mitigated by establishing shorter communication distances when leveraging dense SBSs deployments, reconfigurable intelligent surfacess (RISs), or multi-hop links.

link. Consequently, the total path loss affecting the transmitted signal between the SBS and the VR user will be given by [31]:

$$L(f,r) = L_s(f,r)L_m(f,r) = \left(\frac{4\pi f r}{c}\right)^2 \frac{1}{\tau(f,r)}, \quad (2)$$

where $L_s(f,r) = (\frac{4\pi f r}{c})^2$ is the free-space propagation loss, $L_m(f,r) = \frac{1}{\tau(f,r)}$ is the molecular absorption loss, f is the operating frequency, r is the distance between the VR user and the SBS, c is the speed of light, and $\tau(f,r)$ is the transmittance of the medium following the Beer-Lambert law, i.e., $\tau(f,r) \approx \exp(-K(f)r)$, where $K(f)$ is the overall absorption coefficient of the medium. For sub-THz frequencies $(0.1 - 0.275\,\text{THz})$ $K(f)$ can be calculated using the model suggested by [38]. Meanwhile, for frequencies higher than $0.275\,\text{THz}$, $K(f)$ can be obtained from the high resolution transmission (HITRAN) database [39]. Let $\boldsymbol{p} \triangleq (p_i)_{i=0,1,\cdots,M}$ be a row vector, where p_0 represents the transmission power of the SBS servicing the considered VR user, and p_i represents the transmission power of the interference from any other SBS $i \in \mathcal{M}$. The total noise power is the sum of the molecular absorption noise and the Johnson-Nyquist noise generated by thermal agitation of electrons in conductors. Consequently, the total noise power at the receiver can be given by [31]: $N(\boldsymbol{r}, p_i, f) = N_0 + \sum_{i=1}^{M} p_i A_o r_i^{-2}(1 - e^{-K(f)r_i})$, where $N_0 = \frac{W\lambda^2}{4\pi} k_B T_0 + p_0 A_0 r_0^{-2}(1 - e^{-K(f)r_0})$, k_B is the Boltzmann constant, T_0 is the temperature in Kelvin, and $A_0 = \frac{c^2}{16\pi^2 f^2}$ [29], [40]. By accounting for the total path loss affecting the transmitted signal and considering the M backlogged SBSs in the region of non-negligible interference, the aggregate interference will be [31]: $I(\boldsymbol{r}, p_i, f) = \sum_{i=1}^{M} p_i A_o r_i^{-2} e^{-K(f)r_i}$. The instantaneous frequency-dependent SINR at LoS will be: $S_L(\boldsymbol{r}, \boldsymbol{p}, f) = \frac{p_0^{\text{RX}}(r_0, p_0, f)}{I(\boldsymbol{r}, p_i, f) + N(\boldsymbol{r}, p_i, f)}$, where p_0^{RX} is the received power at the VR user from its associated SBS. Substituting each of the received power, noise, and interference terms results in the following SINR:

$$S_L(\boldsymbol{r}, \boldsymbol{p}, f) = \frac{p_0 A_0 r_0^{-2} e^{-K(f)r_0}}{N_0 + \sum_{i=1}^{M} p_i A_o r_i^{-2}}. \quad (3)$$

Furthermore, our model adopts a single-carrier waveform due to the worsening of the high peak-to-average power ratio (PAPR) problem of orthogonal frequency division multiplexing (OFDM) at THz bands [41]. Also, we consider narrow beamforming and, thus, the delay spread is significantly reduced, and the coherence bandwidth will increase. Hence, similarly to [6], [42], [43] and for tractability, the *achievable* instantaneous rate with an available LoS link is given by:

$$C_L(\boldsymbol{r}, \boldsymbol{p}, f) = W \log_2\left(1 + \frac{p_0 A_0 r_0^{-2} e^{-K(f)r_0}}{N_0 + \sum_{i=1}^{M} p_i A_o r_i^{-2}}\right), \quad (4)$$

where W is the bandwidth. Here, we can see that the only random factor is the second term in the denominator which corresponds to the interfering signals. For technical tractability, following [31], we assume that this term tends to a normal distribution [44]. Indeed, it has been shown in [31] that such an approximation is realistic. Also, finding the mean and variance of this term will allow us to characterize the PDF of this random interference signal, as follows: $g(I) = \frac{1}{\sqrt{2\pi}\sigma_I} \exp\left(-\frac{(I-\mu_I)^2}{2\sigma_I^2}\right)$, where μ_I and σ_I^2 are the mean and variance of the interference, respectively, given by [31]: $\mu_I = pA_0\left(\frac{\ln(\Omega) - \ln(\epsilon)}{\Omega^2 - \epsilon^2}\right)\left(\frac{\pi\Omega^2\eta}{2}\right)$, and $\sigma_I^2 = (pA_0)^2\left(\frac{\pi\Omega^2\eta}{2}\right)\left(\frac{1}{2\epsilon^2\Omega^2}\right)$. Subsequently, the total instantaneous achievable rate is given by: $C_T = P(\Lambda)C_L + P(1-\Lambda)C_N \approxeq P(\Lambda)C_L$. Here, C_N is the rate of the NLoS link and $P(\Lambda)$ is the probability of an available LoS link between the SBS and the VR user. This approximation is based on the significant gap between the power of LoS and NLoS links. $P(\Lambda)$ is fundamental in our analysis given that it can degrade the rate and affect the QoE of the VR users. Given the probabilities of static and dynamic blockages, in Section III, the probability of LoS will be derived in terms of the network parameters.

Next, we analyze whether this network can provide HR2LLC guaranteeing the dual VR requirement. In fact, the rate requirement can easily be achieved by leveraging the large THz bandwidth, however, the reliability remains unclear. To scrutinize the performance of the THz reliability in terms of the E2E delay, we rigorously characterize the distribution of *its tail*, thus, outlining the worst-case performance. Then, we leverage analysis of delay moments to derive the tail distribution and its TVaR.

III. Reliability Analysis

In this section, we examine the probability of blockage and use it to derive the tail distribution of the E2E delay. Furthermore, we evaluate the TVaR of the E2E delay to scrutinize the risks pertaining to an unreliable VR experience at the THz band.

A. Blockage Analysis

Given the electromagnetic properties of THz and its susceptibility to blockage, guaranteeing a LoS path link is necessary to provide a high rate. Therefore, we next quantify the probability of an available LoS link in terms of the channel parameters, thus, characterizing the conditions needed to boost the QoE of the user, as follows:

Proposition 1. In the considered network, the probability of LoS is given by:

$$P(\Lambda) = 1 - \exp\left(\varkappa \aleph \eta_P \pi \Omega^2\right), \quad (5)$$

where Λ is the event of having a LoS path, and $\aleph = \frac{2\left(\nu^2 \ln\left(|\Delta\Omega + \nu|\right) - \nu^2 \ln\left(|\nu|\right)\right)}{\Delta^2\Omega^2} - \frac{2\nu}{\Delta\Omega}$.

Proof: See Appendix A. ∎

The probability of LoS in (5) captures the susceptibility of the THz links to blockage as an exponential function of the network parameters. We observe that an increase in the density of the VR blockers or in the region of blockage affects negatively the availability of LoS. Also, the bigger the sector of the disc of self-blockage, the lower the availability of LoS.

This article has been accepted for publication in a future issue of this journal, but has not been fully edited. Content may change prior to final publication. Citation information: DOI 10.1109/JIOT.2022.3142674, IEEE Internet of Things Journal

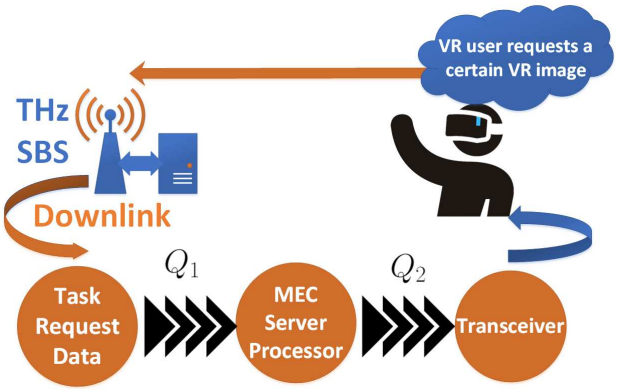

Figure 2: Illustrative example of our queuing model.

B. Delay Analysis

1) Queuing Analysis: Our service model of the VR content request is illustrated in Fig. 2. Here, once a VR user requests a new VR content, it goes through two queues: A first queue, Q_1, for processing a 360° VR content, and a second queue, Q_2, for storing and transmitting the VR content over the wireless THz channel. In particular, Q_1's processing tasks comprise rendering the VR content to be to be viewable on an head-mounted display (HMD). In other words, the MEC processor needs to perform projective transformation operations to render and reverse-project the VR content [45]. Also, the MEC processor needs to process the virtual haptic feedback received by the VR user. Subsequently, it will render this haptic feedback so that the VR user experiences different vibrations and forces while using the VR gloves. We assume a negligible time for sending a request by VR user. Hence, for each VR content request, the total delay depends on the waiting and the processing time at Q_1 and the waiting time and VR transmission delay at Q_2. We consider a Poisson arrival process for the VR content requests with mean rate λ_1. The buffer of the processor is assumed to be of infinite size and the MEC processor at the SBS adopts a first-come, first-serve (FCFS) policy. The service time for each request follows an exponential distribution with rate parameter $\mu_1 > \lambda_1$, to guarantee the stability of the first queue Q_1. Thus, we can model queue Q_1 as an M/M/1 queue. This model can reasonably capture the computation of tasks, as well as the mobility of users requesting VR content [46]. According to Burke's theorem [47], when the service rate is larger than the arrival rate for an M/M/1 queue[4], then the departure process at steady state is a Poisson process with the same arrival rate. Hence, the arrival of requests to Q_2 also follows a Poisson process with rate $\lambda_2 = \mu_1$. Similar to Q_1, we assume an infinite buffer size and an FCFS policy for Q_2. The service time of Q_2 is *the transmission time of the SBS*, that depends on the random wireless THz channel, i.e., the size of the VR content, the LoS rate, and its associated probability of LoS. Thus, different from Q_1, Q_2 is an M/G/1 queue. Our goal is to study when and how our proposed system can guarantee the dual HR2LLC QoS requirements of VR, i.e. visual and haptic perceptions. This dual specification requires a high data rate link for visual perception and a low latency communication for the haptic. Under favorable channel conditions, THz can provide high rate links, however, providing HR2LLC may be challenging. Hence, our key step is to define the system *reliability* and study the fundamental performance of the VR network in terms of HR2LLC requirements. This fundamental performance analysis will shed light on the capability of THz to provide a dual-metric performance for VR: high rate and high reliability.

In our system, reliability cannot be defined merely on average values of delays as done in [2] and [15]. Given the stringent requirements of VR services, a full view on the statistics of the delay must be taken into account to design a system capable of withstanding extreme and infrequently occurring events such as a sudden user movement or a sudden blockage event which can impact reliability. To analyze reliability, next, we derive the moments of the E2E delay and use them to derive the tail distribution of the E2E delay. Based on the expression of the tail distribution, the TVaR will be derived to characterize the value of the E2E delay at the tail, in the presence of a risk of an unreliable user experience.

2) Tail Reliability Analysis: Fundamentally, to guarantee reliability in the face of stochastic and dynamic wireless channels, its is necessary to analyze the *instantaneous* behavior of the network rather than its average [48]. Furthermore, it is necessary to examine any *instantaneous* exceedance of the E2E delay above a threshold that disrupts the user QoS. Since VR services call for *perceptual and haptic* requirements directly linked to the user QoE; we define *the reliability of the VR system* as a guarantee that the instantaneous E2E delay can be maintained below a target threshold δ. Formally and according to 3GPP [5], reliability is defined as the capability of transmitting a given amount of traffic within a predetermined time duration with high success probability. However, given that our traffic consists of VR content that needs more stringent reliability measures to ensure a seamless experience, we fortify that statement and make it more stringent by *defining reliability as the probability that the E2E delay – defined as the delay incurred between the time the VR user requests a VR image to the time the image is received – remains below a stringent threshold* δ. Here, central statistical characteristics of the E2E delay such as the average or median performance do not guarantee a *continuously reliable system*. Meanwhile, shifting our focus to extreme values of the E2E delay and their corresponding limiting distribution allows us to guarantee a highly reliable system under very difficult conditions. In other words, analyzing the behavior of E2E *tail* delay distributions is suited to capture the reliability response vis-à-vis the worst-case conditions, i.e., tail analysis will guarantee high reliability for a user experiencing a deep fade or a sudden blockage. Thus, this guarantees an *instantaneous and continuously reliable THz system*. Subsequently, we leverage the renowned EVT framework [27] to capture the behavior of the tails and

[4]In our model, the processing unit's speed is significantly higher than the VR content's request

This article has been accepted for publication in a future issue of this journal, but has not been fully edited. Content may change prior to final publication. Citation information: DOI 10.1109/JIOT.2022.3142674, IEEE Internet of Things Journal

extreme statistics of interest. In particular, we leverage block maxima EVT models whose data points tend to be measured over a particular period of time (e.g. VR session time in our case) and tend to be time-sensitive. Consequently, the EVT theorem is formally defined as:

Definition 1. (Fisher–Tippett–Gnedenko theorem [49]) Given a sequence of i.i.d. variables $\{x_1, \ldots, x_n\}$, the distribution of $M_n = \max\{x_1, \ldots, x_n\}$ representing the maximum value of the sequence converges (for large n) toward the generalized extreme value (GEV) characterized by the following CDF and PDF:

$$F_E(x;\xi_E) = \begin{cases} \exp\Big(-(1+\xi_E \frac{x-\mu_E}{\sigma_E})^{-1/\xi_E}\Big), & \xi_E \neq 0, \\ \exp\Big(-\exp\Big(-\frac{x-\mu_E}{\sigma_E}\Big)\Big), & \xi_E = 0\ , \end{cases} \tag{6}$$

where ξ_E is the shape parameter, μ_E the location parameter, and $\sigma_E \geq 0$ is the scale parameter Thus for $\xi > 0$, the expression is valid for $\frac{x-\mu_E}{\sigma_E} > -1/\xi$, while for $\xi < 0$ it is valid for $\frac{x-\mu_E}{\sigma_E} < -1/\xi$.

$$f_E(x) = \begin{cases} (1+\xi_E)^{(-1/\xi_E)-1} \exp\Big(-(1+\xi_E \frac{x-\mu_E}{\sigma_E})^{-1/\xi_E}\Big), \xi_E \neq 0, \\ \exp\Big(-\frac{x-\mu_E}{\sigma_E}\Big) \exp\Big(-\exp\Big(-\frac{x-\mu_E}{\sigma_E}\Big)\Big), \xi_E = 0. \end{cases} \tag{7}$$

In our model, the sequence of i.i.d. variables corresponds to the sequence of E2E delays experienced by the VR user; subsequently, this theorem paves the way to characterize the distribution of the maximum E2E delay that a VR user can experience, and hence the worst-case scenario. Consequently, next, we perform moment matching to match the moments of the GEV distribution to those of the moments of the E2E delay over our THz network. First, for our model in Fig. 2, given that Q_1 is an M/M/1 queue, the mean of the total waiting time at Q_1 will be $\mathbb{E}[T_1] = \frac{1}{\mu_1 - \lambda_1}$. Moreover, given that Q_2 is an M/G/1 queue, the mean of the total waiting time is given by:

$$\mathbb{E}[T_2] = \left[\left(\frac{\rho_2}{1-\rho_2}\frac{C_\alpha^2+1}{2}\right)+1\right]\mathbb{E}[\alpha], \tag{8}$$

where $\rho_2 = \frac{\lambda_2}{\mu_2}$ is the queue utilization, α is the transmission delay, and $C_\alpha^2 = \frac{\vartheta(\alpha)}{E^2[\alpha]}$ is the squared coefficient of variation. Next, we evaluate the mean of the E2E delay. This mean constitutes the first moment, that is then used to perform a moment matching between our empirical E2E delay moments and the GEV distribution, to finally characterize the tail distribution. Note that this characterization has not been done in any prior work [6], [21]–[23], [50].

Theorem 1. *The mean of the E2E delay is given by:*

$$\mathbb{E}[T_1{+}T_2] = \frac{1}{\mu_1-\lambda_1} + \mathbb{E}[\alpha]\left[1+\left(\frac{\rho_2}{2(1-\rho_2)}\times \left(\frac{1}{\left(W\log_2\left(1+\frac{p_0 A_0 r_0^{-2} e^{-K(f)r_0}}{N_0+\mu_I}\right)\right)^2}V_a(Z)+1\right)\right)\right], \tag{9}$$

where

$$\mathbb{E}[\alpha] \approx \frac{L}{\left(1-\left(\frac{e^{\pi Z}-1}{\pi Z}\right)\right)\left(W\log_2\left(1+\frac{p_0 A_0 r_0^{-2} e^{-K(f)r_0}}{N_0+\mu_I}\right)\right)}, \tag{10}$$

$$Z = \aleph \eta_P \Omega^2. \tag{11}$$

Proof: See Appendix B. ∎

From (9), we can see that the average E2E delay is equally influenced by the mean of the total waiting time in Q_1, the utilization of Q_2, and the mean of the transmission delay α (and thus the THz environment). The waiting time in Q_1 is mainly influenced by the number of VR requests and the processing speed of the MEC server, which are beyond the control of the wireless network. Meanwhile, the transmission delay depends on the average blockage rate (which in turn is the complement of $P(\Lambda)$ derived in (5) in Proposition 1) and the average THz data rate. Clearly, the density of VR users, their mobility, and their requests for VR content all play a role in the average behavior of the network. Next, we derive the second moment of the E2E delay, thus allowing us later to capture the GEV of the E2E delay and examine the instantaneous E2E delay and its consequent effect on the QoE.

Lemma 1. *The second moment of the E2E delay is given by:*

$$\begin{aligned}\mathbb{E}[(T_1{+}T_2)^2] = {} & \left(\frac{2}{\mu_1-\lambda_1}\right)\mathbb{E}[\alpha]\left[1+\left(\frac{\rho_2}{2(1-\rho_2)}\times \left(\frac{1}{\left(W\log_2\left(1+\frac{p_0 A_0 r_0^{-2} e^{-K(f)r_0}}{N_0+\mu_I}\right)\right)^2}V_a(Z)+1\right)\right)\right] \\ & + \frac{2}{(\mu_1-\lambda_1)^2} + \mathbb{E}[\alpha^2] + \frac{\rho_2\mathbb{E}[\alpha^3]}{3(1-\rho_2)} + \frac{\rho_2\mathbb{E}[\alpha^2]}{2(1-\rho_2)} \\ & + \left[\left(\frac{\rho_2}{2(1-\rho_2)}\right)\left(\frac{\mathbb{E}[\alpha^2]}{\mathbb{E}[\alpha]}\right)\right]^2. \end{aligned} \tag{12}$$

Proof: See Appendix C. ∎

Having the first and second moment in (9) and (12) of the E2E delay allows us to derive the moments of the highest order statistics of the E2E delay to finally characterize the tail distribution. To do so, in what follows, we first order the set of E2E delays and arrange them in an increasing order of magnitude. Subsequently, we model the tail of the E2E delay to be the highest order statistic, i.e., the maximum of the set. Given that we have obtained the first and second moments of the parent distribution of the E2E delay, we need to express the first and second moments of the highest order statistic in terms of the expectations formulated in Theorem 1 and Lemma 1. Thus, from [51], given the mean and variance of the parent distribution, we can find the highest order statistics expectation as:

$$\mathbb{E}[(T_1+T_2)_n] \approxeq \mathbb{E}[(T_1+T_2)] + \frac{(n-1)\left(\vartheta(T_1+T_2)\right)^{\frac{1}{2}}}{(2n-1)^{1/2}}. \tag{13}$$

Given (13), next, we characterize the GEV distribution of the tail after performing a moment matching and deriving its defining parameters.

This article has been accepted for publication in a future issue of this journal, but has not been fully edited. Content may change prior to final publication. Citation information: DOI 10.1109/JIOT.2022.3142674, IEEE Internet of Things Journal

Theorem 2. *The tail distribution of the E2E delay follows a GEV distribution with a location, scale and shape parameter given by:*

$$\mu_E = \frac{1}{\mu_1-\lambda_1} + \mathbb{E}[\alpha]\left[1+\left(\frac{\rho_2}{2(1-\rho_2)}\times \left(\frac{1}{\left(W\log_2\left(1+\frac{p_0 A_0 r_0^{-2} e^{-K(f)r_0}}{N_0+\mu_I}\right)\right)^2}V_a(Z)+1\right)\right)\right], \tag{14}$$

$$\sigma_E^2 = \frac{1}{\mu_1-\lambda_1} + \mathbb{E}[\alpha^2] + \frac{\rho_2\mathbb{E}[\alpha^3]}{3(1-\rho_2)} + \frac{\rho_2\mathbb{E}[\alpha^2]}{2(1-\rho_2)} + \left[\left(\frac{\rho_2}{2(1-\rho_2)}\right)\left(\frac{\mathbb{E}[\alpha^2]}{\mathbb{E}[\alpha]}\right)\right]^2 - \left(\mathbb{E}[\alpha]\left[1+\left(\frac{\rho_2}{2(1-\rho_2)}\times \left(\frac{1}{\left(W\log_2\left(1+\frac{p_0 A_0 r_0^{-2} e^{-K(f)r_0}}{N_0+\mu_I}\right)\right)^2}V_a(Z)+1\right)\right)\right]\right)^2, \tag{15}$$

$$\frac{\xi_E}{\Gamma(1-\xi_E)-1} = \frac{(2n-1)^{1/2}}{(n-1)}. \tag{16}$$

Proof: See Appendix D. ∎

Theorem 2 allows us to tractably characterize the tail of the distribution E2E , i.e., the worst case distribution over all of the possible outcomes of randomness rather than just an average value. Moreover, interestingly the tail distribution's location μ_E is the average of the E2E delay. Thus, the distribution of the tail of the E2E delay is centered around the mean of the E2E delay. Moreover, the scale of the distribution is the variance of the E2E delay. Clearly, the tail variance is highly influenced by the first three moments of the THz data rate, thus characterizing the susceptible THz behavior to the dynamic environment. As for the shape, it depends on the number of VR requests in each VR session. Therefore, the moments of the E2E delay mirror variations of lower order statistics to obtain the highest order statistic distribution. By obtaining the tail statistics and its distribution, we can further quantify the E2E delay value given a specific level of risk of unreliable experience. In other words, we *define the notion of risk based on its confidence level*: a confidence level of 99% means that we are 99% sure that the worst-case delay will not exceed a specific value. Clearly, examining tail distributions not only characterizes the worst-case scenario but also provides guarantees through risk measures, thus providing more leverage for HR2LLC. To formulate these risk measures, in actuarial sciences, the value-at-risk (VaR) concept is defined as a quantile of the distribution of aggregate losses, $\text{VaR}_{1-\alpha} = -\inf_{t\in\mathbb{R}}\{P(X \le t) \ge 1-\alpha\}$ [27]. However, VaR is an incoherent[5] and intractable risk measure. TVaR, on the other hand, is defined as the expected loss conditioned on the loss exceeding the VaR [52]. Thus, TVaR not only measures the risk but also quantifies its severity, making it a superior risk measure. In our context, the TVaR allows us to scrutinize the tail of the E2E delay, at a given confidence level. Thus, if the instantaneous E2E delay follows a PDF $\Phi(t)$, such that the E2E delay does not exceed a certain threshold γ, we can define the risk of an unreliable QoE to be related to the VaR as follows: $\int_\gamma^\infty \Phi(t)dt = 1-\alpha_C$, where $\text{VaR}(\alpha_C) = \gamma$. Subsequently, we define χ to be the right-tail TVaR to be defined as: $\chi = \frac{1}{1-\alpha_c}\int_\gamma^\infty t\Phi(t)dt$. Given our knowledge about the GEV distribution, the TVaR for our network can be formally derived next (following directly from Theorem 2).

[5]A coherent risk measure is a metric that satisfies properties of monotonicity, sub-additivity, homogeneity, and translational invariance.

Corollary 1. *The TVaR of the E2E delay T_e is given by:*

$$\chi = \mu_E + \frac{\sigma_E}{(1-\alpha_C)\xi_E}\left[\gamma\left(1-\xi_E, -\log(\alpha_C)\right) - (1-\alpha_C)\right], = \mathbb{E}[T_e] + \frac{(\vartheta(T_e))^{\frac{1}{2}}}{(1-\alpha_C)\xi_E}\left[\gamma\left(1-\xi_E, -\log(\alpha_C)\right) - (1-\alpha_C)\right], \tag{17}$$

where γ is the lower incomplete gamma function defined by $\gamma(s,x) = \int_0^x t^{s-1}\,\mathrm{e}^{-t}\,\mathrm{d}t$

As seen from (17), the TVaR is a tractable expression that is a function of the first and second moment of the E2E delay. These moments bring to view the fastness and robustness of THz frequency bands and the MEC server in a dynamic VR environment. Based on these moments, the TVaR provides us with the expected E2E delay conditioned on the E2E delay exceeding a specific threshold. In other words, it helps shed light on the severity of exceeding the threshold, by quantifying the expectation of the tail distribution. Considering the TVaR allows us to provide the user a seamless experience with a reliability in the order of its confidence level. A confidence level of α_C guarantees the maximum E2E delay to be below that threshold, α_Cth of the time.

Next, we perform an asymptotic analysis for reliability under idealized conditions in which we assume the probability of LoS to be equal to 1.

IV. Reliability for Scenarios with Guaranteed LoS

Hereinafter, we assume the probability of LoS to be equal to 1, i.e., a continuous LoS is available to the VR user. Thus, this facilitates our model further making it feasible to analyze true CDFs and PDFs of the delay instead of relying on tail distributions. This special case scenario is meaningful given that it portrays cases where the number of active VR users is significantly low in the indoor area and where the user's orientation does not vary rapidly. Subsequently, for our model in Fig. 2, given that Q_1 is an M/M/1 queue, the PDF of the total waiting time at Q_1 will be [47]:

$$\psi_1(t) = (\mu_1-\lambda_1)\exp\left(-(\mu_1-\lambda_1)t\right). \tag{18}$$

Given that Q_2 is an M/G/1 queue and that the queuing and service time of an M/G/1 queue are independent, we find the CDF of the total waiting time: $\Psi_2(t) = \Psi_{Q_2}(t) * \psi_T(t)$, where $*$ is the convolution operator, $\Psi_{Q_2}(t)$ is the CDF of the

This article has been accepted for publication in a future issue of this journal, but has not been fully edited. Content may change prior to final publication. Citation information: DOI 10.1109/JIOT.2022.3142674, IEEE Internet of Things Journal

Table II: Simulation parameters based on typical values.

Parameters	Values	Parameters	Values
Carrier Frequency f	$\{0.2\,\text{THz}, 1\,\text{THz}\}$	Number of VR users V	50
Noise power spectrum density at UE σ^2	-174 dBm/Hz	Molecular absorption coefficient $K(f)$	$\{2.10^{-4}\text{m}^{-1}, 0.0016\,\text{m}^{-1}\}$
Transmit power at SBS p	30 dBm	VR content packet size L	10 Mbits
Density of SBSs η	$\{0.06\,\text{m}^{-1}, 0.25\,\text{m}^{-1}\}$	Water vapor percentage	1 %
Request arrival rate at Q_1 λ_1	0.1 packets/s	Computing service rate at Q_1 μ_1	{14 Gbps, 19 Gbps} effective
Velocity of dynamic blockers v_B	1.5 m/s	Arrival rate to blockage queue κ_B	2 blockers/s

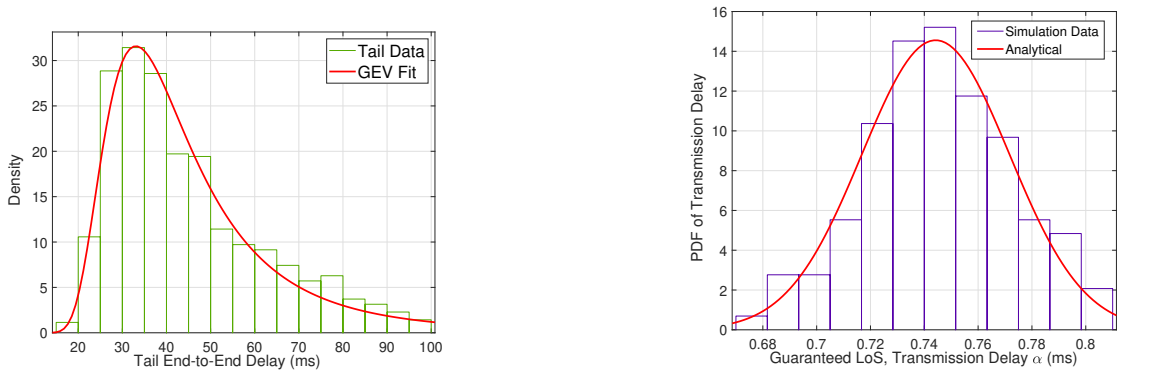

(a) (b)

Figure 3: (a) PDF fit of the tail end-to-end delay, (b) PDF fit of the transmission delay (Guaranteed LoS Scenario).

queuing time at Q_2 and $\psi_T(t)$ is the PDF of the transmission delay. The CDF of the total queuing time at Q_2 will be [47]:

$$\Psi_{Q_2(t)} = (1-\rho_2)\sum_{n=0}^{\Gamma}\left[\rho_2^n R^{(n)}(t)\right]. \tag{19}$$

Here, Γ is the number of states that the queue has went through, i.e., the number of packets that has passed through the queue during a certain amount of time and $R^{(n)}(t)$ is the CDF of the residual service time after the n-th state. Note that $R^{(n)}(t)$ can be computed by obtaining the residual service time distribution $R(t)$ after n packets, $R(t) = \int_0^t \mu_2(1-\psi_T(x))dx$, where t is the time of an arbitrary arrival, given that the arrival occurs when the server is busy. To evaluate the PDF of the E2E delay, we need the PDF of the transmission delay which is found next:

Lemma 2. *The PDF of the transmission delay is given by:*

$$\psi_T(\alpha) = \frac{\zeta}{\sqrt{2\pi}\sigma_I}\exp\left(-\frac{(\Upsilon-\mu_I)^2}{2\sigma_I^2}\right), \tag{20}$$

where

$$\zeta = \frac{\ln(2)(p_0^{RX}L)2^{\frac{L}{W\alpha}}}{W\alpha^2(2^{\frac{L}{W\alpha}}-1)^2}, \qquad \Upsilon = \frac{(1-2^{\frac{L}{W\alpha}})N_0 + p_0^{RX}}{2^{\frac{L}{W\alpha}}-1},$$

Proof: See Appendix E. ∎

It is important to note that the PDF in (20) does not follow a normal distribution since both Υ and ζ depend on the transmission delay α. Burke's Theorem allows us to infer that Q_1 and Q_2 are independent, and, thus, the CDF of the E2E delay can be expressed as the convolution of the PDF of the total waiting time in Q_1 and the CDF of the total waiting time in Q_2. By using the dynamics in (18) and (19), the CDF of the E2E delay can formally expressed in the following theorem which is a direct result of Lemma 2.

Theorem 3. *The CDF of the E2E delay T_e is given by:*

$$\Phi(t) = P(T_e \le t) = \psi_1(t) * \Psi_2(t) = \psi_1(t) * (\Psi_{Q_2}(t) * \psi_T(t))$$
$$= (\mu_1-\lambda_1)\exp(-(\mu_1-\lambda_1)t)$$
$$* \left((1-\rho)\sum_{n=0}^{\Gamma}(\rho^{\Gamma}R^{(n)}(t))\right) * \left(\frac{\zeta}{\sqrt{2\pi}\sigma_I}\exp\left(-\frac{(\Upsilon-\mu_I)^2}{2\sigma_I^2}\right)\right). \tag{21}$$

Consequently, the *reliability* with respect to a certain threshold δ, is given by:

$$\varrho = P(T_e \le \delta) = \Phi(\delta). \tag{22}$$

The reliability defined in (22) provides a tractable characterization of the reliability of the VR system shown in Fig. 1, as function of the THz channel parameters. For instance, from Theorem 3, we can first observe that the queuing time of Q_2 depends on the residual service time CDF and, thus, on the transmission delay. Also, given that the processing speed of a MEC server can be considerably high, the E2E delay will often be dominated by the transmission delay over the THz channel. In general, all the key parameters that have a high impact on the transmission delay will have a higher impact on reliability. One of the most important key parameters is the distance r_0 between the VR user and its respective SBS; this follows from the fact that the molecular absorption loss gets significantly higher when the distance increases, which limits the communication range of THz SBSs to very few meters. Indeed, the THz reliability will deteriorate drastically if the distance

This article has been accepted for publication in a future issue of this journal, but has not been fully edited. Content may change prior to final publication. Citation information: DOI 10.1109/JIOT.2022.3142674, IEEE Internet of Things Journal

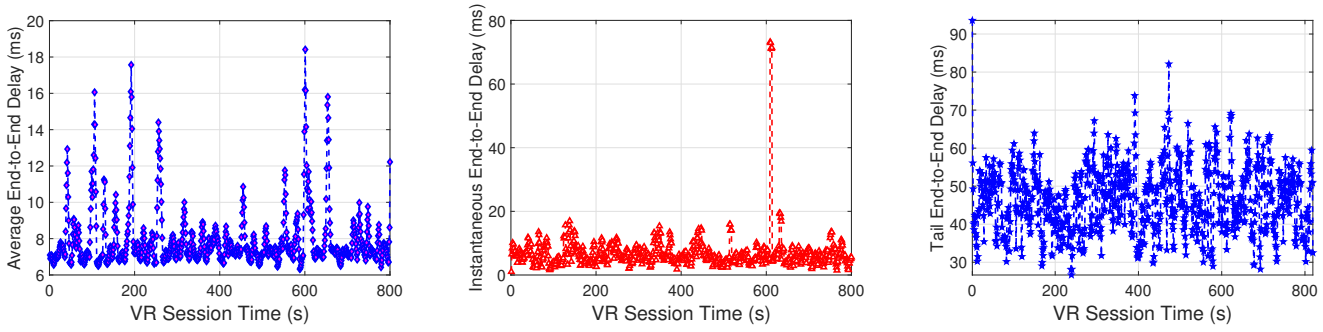

(a) (b) (c)

Figure 4: THz Performance over a VR Session ($f = 1\,\text{THz}$) (a) Average E2E delay versus VR session time, (b) Instantaneous E2E delay versus VR session time, (c) Tail E2E delay versus VR session time.

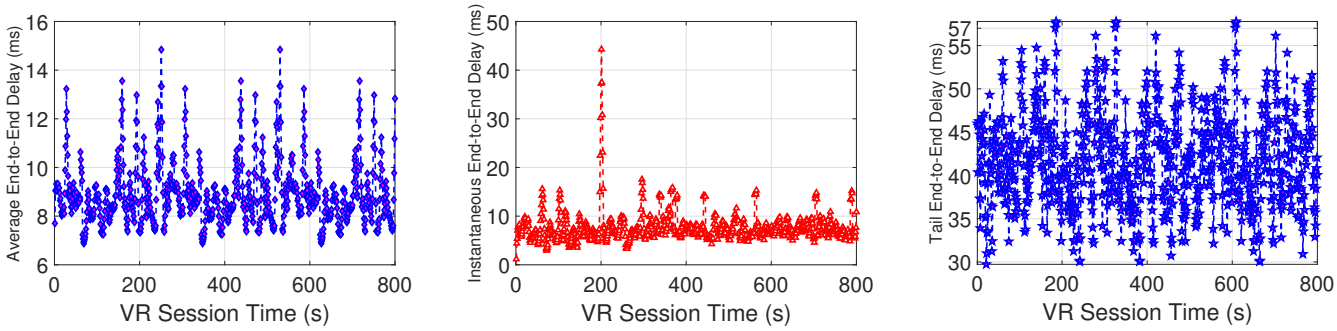

(a) (b) (c)

Figure 5: Sub-THz Performance over a VR Session ($f = 0.2\,\text{THz}$) (a) Average E2E delay versus VR session time, (b) Instantaneous E2E delay versus VR session time, (c) Tail E2E delay versus VR session time.

between the VR user and its respective SBS increased. Also, in this special case, the PDF of the E2E delay is tractable. Thus, providing the full statistics of the E2E delay without having to examine averages and tails to scrutinize the risks pertaining to reliability. In other words, the PDF of the E2E delay provides us with generalizable information, reflecting the overall behavior of reliability in this model. Hence, while the tail reliability analyzed in Section III is mostly threatened by the probability of blockage, in this scenario, the challenges that need to be addressed to provide a robust reliability are the short communication range as result of the molecular absorption effect, and the interference stemming from the high network density. Moreover, given the QoS of a VR application is a function of the reliability, i.e., it is the reliability of the system throughout the worst case scenario. VR users' immersion and experience will depend significantly on the reliability. Therefore, maintaining reliability is a necessary condition to guarantee the QoS for the user, thus increasing its satisfaction and yielding it a seamless experience.

V. Simulation Results and Analysis

For our simulations, we consider a setting in which VR users are receiving VR content as they engage in a VR video game (Star Wars: Squadrons). The SBSs are deployed in an indoor area modeled as a square of size $20\,\text{m} \times 20\,\text{m}$ at $T = 300\,\text{K}$. All statistical results are averaged over $2,500$ independent runs. The main simulation parameters are shown in Table II. The molecular absorption coefficient was obtained using the HITRAN database for $1\,\text{THz}$ and using the sub-THz model [38] for $0.2\,\text{THz}$. The processing rate of Q_1 is chosen to comply with existing VR processing units such as the GeForce RTX 3080 and GEFORCE RTX 2080 Ti [53], [54]. Next, we compare how the *realistic scenario, i.e., when considering blockages* in Section II, contrasts with the asymptotic analysis we have performed in Section IV where LoS is always guaranteed.

Fig. 3a shows that the simulation results match the distribution of the analytical result derived of Theorem 2. The small mismatch between the analytical and simulation results stems from the use of Jensen's inequality. Clearly, the tail of E2E delay is centered around $40\,\text{ms}$, but can reach up to $100\,\text{ms}$. Moreover, Fig. 3b shows that the simulation results match the distribution of the analytical result derived in Lemma 2. The small gap between the analytical and simulation results stems from the use of the normal distribution assumption for the interference. Fig. 3b shows how the transmission delay is low, i.e., it is centered at $0.75\,\text{ms}$, owing to the high data rates at THz frequency bands.

Fig. 4 shows how the average, instantaneous, and tail E2E delays experienced by the user during a VR session, vary, respectively for a carrier frequency of $f = 1\,\text{THz}$. Clearly, the average E2E delay provides a positive viewpoint of the

This article has been accepted for publication in a future issue of this journal, but has not been fully edited. Content may change prior to final publication. Citation information: DOI 10.1109/JIOT.2022.3142674, IEEE Internet of Things Journal

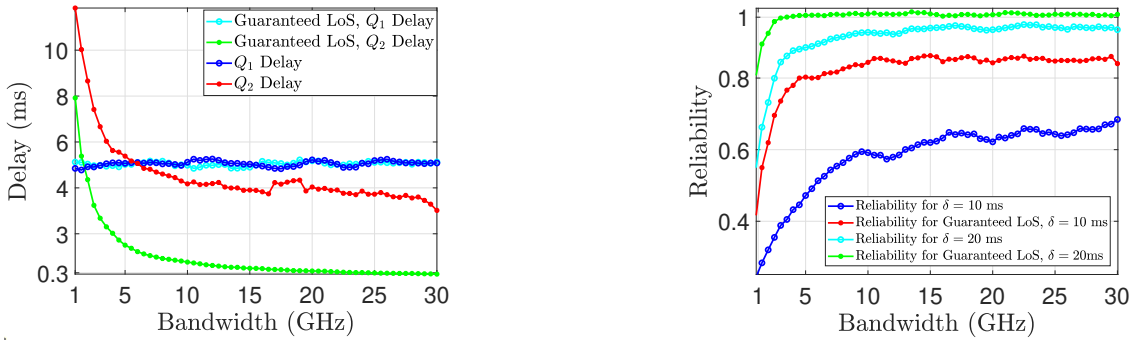

(a) (b)

Figure 6: Effect of bandwidth on the achievable THz performance ($f = 1\,\text{THz}$) (a) Delay versus bandwidth, (b) TVaR versus bandwidth.

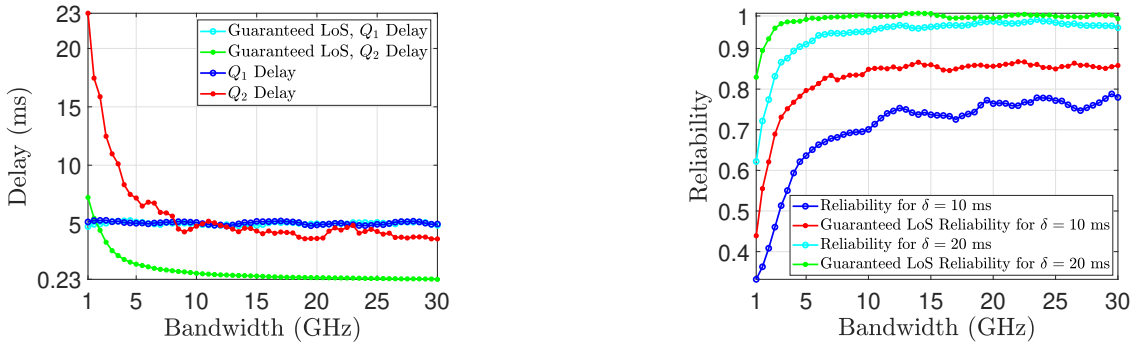

(a) (b)

Figure 7: Effect of bandwidth on the achievable sub-THz performance ($f = 0.2\,\text{THz}$) (a) Delay versus bandwidth, (b) TVaR versus bandwidth.

reliability of THz, as its upper bound is limited by $20\,\text{ms}$. For the instantaneous E2E delay, we can see how a single extreme event (a sudden self-blockage) throughout the VR session can suddenly disrupt the VR experience. This is why it is important to model the distribution of tails characterizing these extreme events. Fig. 4c shows a negative perspective of reliability, as the tails are lower bounded by an E2E delay of $30\,\text{ms}$, i.e., any extreme event will lead to a minimum E2E delay of $30\,\text{ms}$, thus leading to a sudden disruption of the user's experience. Clearly, Fig. 4 reveals that average designs overlook *extreme events* that disrupt real-time experiences. Hence, it is important to provide solutions that particularly improve the tail performance of THz, given that on average reliability is high.

Similarly to Fig. 4, Fig. 5 characterizes the sub-THz performance of the average, instantaneous, and tail E2E delays at a carrier frequency of $f = 0.2\,\text{THz}$. The sub-THz performance also portrays a positive viewpoint of the reliability of THz, whereby its upper bound is limited by $15\,\text{ms}$. Moreover, the instantaneous E2E delay shows a disruption due to a single extreme event at time $200\,\text{s}$ of the VR session (a dynamic blockage). Interestingly, the upper bound of the average, instantaneous, and tail delay is considerably lower compared to the performance at $f = 1\,\text{THz}$. Meanwhile, the lower bound is higher. This is attributed to the fact that higher bands are characterized by an *all or nothing* behavior. In other words, at higher carrier frequencies, lower transmission delays can be achieved, thus leading to extremely low E2E delays at the lower bounds. Nevertheless, the higher end of the THz frequency bands experiences a higher susceptibility to extreme events, thus contributing to more breaks in the service and heavier tails.

Fig. 6a and Fig. 7a show the prominent effect of the bandwidth on the delays of Q_1 and Q_2, in presence of blockages and for the idealized, guaranteed LoS scenario at THz and sub-THz respectively. We can see that, in both cases, increasing the bandwidth ensures a reliable performance, but remains limited by the processing speed at the MEC server. Nevertheless, considering blockages increases Q_2 delay on average from $0.3\,\text{ms}$ to $4\,\text{ms}$ at a bandwidth of $20\,\text{GHz}$ for THz frequencies, and from $0.23\,\text{ms}$ to $3.5\,\text{ms}$ at a bandwidth of $20\,\text{GHz}$ for sub-THz frequencies. Therefore, in presence of blockage, increasing the bandwidth (up to $30\,\text{GHz}$) is not sufficient to guarantee a high reliability. Interestingly, when increasing the bandwidth at $f = 0.2\,\text{THz}$ the transmission delay sees a more significant change. Thus, changing the bandwidth has a greater impact when the network operates at $f = 0.2\,\text{THz}$ compared to $f = 1\,\text{THz}$. This phenomenon

This article has been accepted for publication in a future issue of this journal, but has not been fully edited. Content may change prior to final publication. Citation information: DOI 10.1109/JIOT.2022.3142674, IEEE Internet of Things Journal

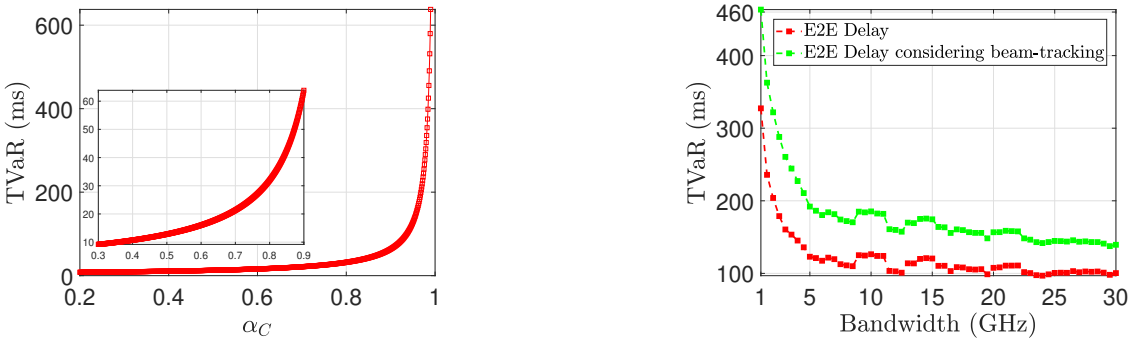

(a) (b)

Figure 8: TVaR Performance (a) TVaR versus α_C, (b) TVaR versus bandwidth with $\alpha_C = 95\,\%$.

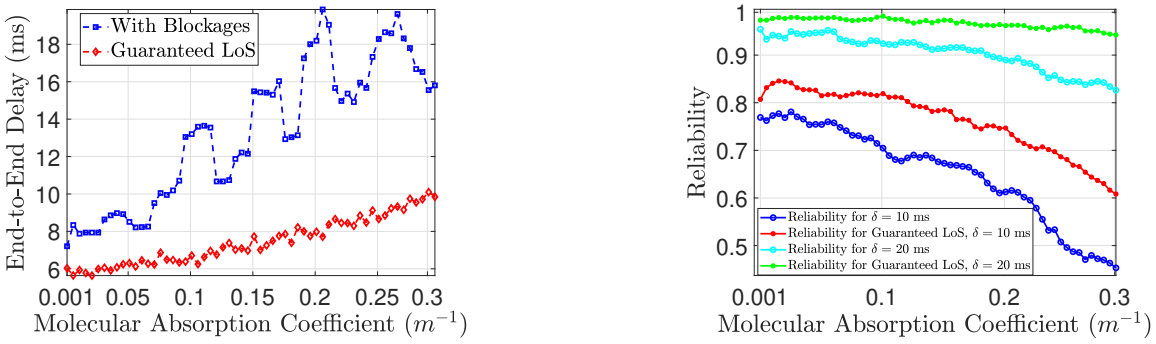

(a) (b)

Figure 9: Effect of molecular absorption on the achievable performance (a) Delay versus molecular absorption coefficient, (b) Reliability versus molecular absorption coefficient.

is observed due to the more pronounced extreme events at higher carrier frequencies. In particular, Fig. 6b shows that the reliability of THz at $f = 1\,\text{THz}$ is limited to 68% and 96% for a target delay of $\delta = 10\,\text{ms}$ and $\delta = 20\,\text{ms}$ at a significant bandwidth of 30 GHz. In contrast, in the guaranteed LoS scenario, we need a bandwidth of $15\,\text{GHz}$ to achieve a reliability of $99.999\,\%$, thus reducing significant spectrum resources when LoS is available, this also corresponds to a data rate of $18.3\,\text{Gbps}$. Meanwhile, at $f = 0.2\,\text{THz}$, the performance is limited to 80% and 98% for a target delay of $\delta = 10\,\text{ms}$ and $\delta = 20\,\text{ms}$ at a bandwidth of $30\,\text{GHz}$. However, this comes at the expense of a lower data rate of $11.5\,\text{Gbps}$.

To assess the reliability of the tails, Fig. 8a shows how the TVaR varies with respect to the confidence level α_C. We can observe that while it is fairly easy to guarantee tail delays with a confidence of 80% at $30\,\text{ms}$, yet it is very difficult to tame low E2E tail delay with a risk percentile above $90\,\%$. In fact, at a confidence level of $99\,\%$, the tail E2E delay becomes as high as $450\,\text{ms}$, compared to $63\,\text{ms}$ at a confidence level of $90\,\%$. Moreover, Fig. 8b shows the effect of bandwidth on the TVaR at a confidence level of $95\,\%$: Clearly, an increased bandwidth reduces the risk of occurrence of extreme events. Nevertheless, given the susceptibility of THz to the dynamic network conditions, increasing the bandwidth remains limited by a best-case TVaR of $100\,\text{ms}$. Additionally, taking into account the beam-tracking delay[6] shows higher values of TVaR. In this case, increasing the bandwidth remains limited by a best-case TVaR of $130\,\text{ms}$.

Fig. 9a shows the effect of the molecular absorption coefficient on the E2E delay, we can see that with a guaranteed LoS, the E2E delay increases monotonically with the molecular absorption. Nevertheless, when blockages are considered, the THz electromagnetic properties make it more susceptible to the dynamic environment as the molecular absorption coefficient increases, thus, increasing the occurrence of signal disruptions and leading to fluctuations as the molecular absorption increases. Moreover, we can see in Fig. 9b that the molecular absorption has a more pronounced effect on the reliability of the system when considering blockages, this is observed regardless of the reliability threshold δ. Clearly, for a threshold $\delta = 10\,\text{ms}$, the availability of LoS improves the reliability by $13\,\%$ (from $70\,\%$ to $83\,\%$).

Fig. 10 shows how the reliability varies as a function of the region of non-negligible interference, in the guaranteed LoS scenario. We can see that, when the distance between the VR user and the SBS increases, the region of non-negligible interference Ω has a higher impact on the reliability, and the drop of reliability is sharper. This phenomenon is

[6]The beam-tracking method adopted is a low overhead technique that combines hierarchical codebook search with a location prediction algorithm, similar to the one in [55].

This article has been accepted for publication in a future issue of this journal, but has not been fully edited. Content may change prior to final publication. Citation information: DOI 10.1109/JIOT.2022.3142674, IEEE Internet of Things Journal

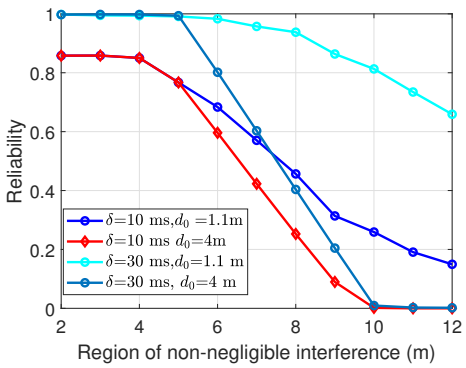

Figure 10: Reliability for Guaranteed LoS versus region of non-negligible interference

observed regardless of the reliability threshold δ. Hence, even though the user can achieve high reliability, the dependence of the molecular absorption on distance limits the user to a very short distance to its respective SBS. Thus, the VR user can be guaranteed reliability regardless of the interference surrounding it, given that it is at a proximity of the respective SBS.

VI. Conclusion

In this paper, we have studied the feasibility of ensuring reliability of VR services in the THz band. To obtain an expression for the E2E delay and reliability, we have proposed a model based on a two tandem queue, in which we have derived the tail distribution of the E2E delay via its lower order moments. Subsequently, we have derived the TVaR of the E2E delay tail, characterizing the worst case scenario. Furthermore, we have conducted an asymptotic analysis where we derived the PDF of the transmission delay of a THz cellular network, based on which, we have derived the E2E delay expression along with the reliability of this system. We particularly have made the following observations regarding the reliability of THz networks:

- While it is necessary to increase the bandwidth and operate at regions of low molecular absorption, e.g., indoor areas, to provide a reliable experience; extreme events resulting from the unavailability of LoS links, disrupt the user's QoE and increase the E2E delay significantly.
- Performance analyses based on the tail of E2E delays are fundamental to characterize the THz performance, given the insights it provides on extreme events. In that regard, guaranteeing a LoS is of primary importance to improve the tail performance. Such a guarantee becomes more challenging in outdoor areas and with highly mobile UE. It is thus necessary to explore directions that optimize, and increase the availability of LoS links in THz. One potential solution could be the deployment of RIS as done in our work in [29]. Another method is to leverage the synergy of THz frequencies with lower frequency bands at the control plane [56].
- Independent from the network architecture, guaranteeing continuous THz LoS links necessitates predicting the user's micro-mobility and micro-orientation at every time step. Having such predictions in hand allows the network operator to mitigate the intermittent nature of THz links. Thus, it significantly improves the system reliability. Henceforth, the artificial intelligence (AI) approaches suggested in [29] and [56] can be extended to our studied model, leading to a promising subject of future work.
- After guaranteeing a LoS availability, the THz reliability remains impeded by factors such as the short communication range due to the molecular absorption effect and the interference arising due to the high network density. Consequently, it is necessary to explore new predictive mechanisms that can handle the large-scale nature of a wireless network and that is reliable in face of high uncertainty and extreme network conditions.
- Similarly to the approach performed in our analysis, considering tails and risks in the analysis of wireless systems is fundamental for *time critical* use cases [57]. Hence, it is important to extend such analyses to use cases like eXtended reality (XR) (VR, augmented reality (AR), mixed reality (MR)), holographic teleporation, and digital twins. Such use cases have slightly different QoS and QoE needs than VR, and thus the performance analysis needs to be tuned accordingly. For instance, in holographic teleportation, one needs to guarantee that the five senses are synchronized instantaneously, i.e., the instantaneous delay stemming from each sense is identical and extremely low.

Appendix

A. Proof of Proposition 1

Proof: Given the probability of simultaneous blockage of all LoS paths, the conditional probability of LoS is given by:

$$P(\Lambda|q,\boldsymbol{r_i}) = 1 - \prod_{i=1}^{q}\left(1 - \varkappa \frac{1}{1+\frac{\Delta}{\nu}r_i}\right). \tag{23}$$

Subsequently, we need to find the marginal probability of one LoS path:

$$\begin{aligned} P(\Lambda|q) &= \iint_{\boldsymbol{r_i}} P(\Lambda|q,\boldsymbol{r_i}) f(\boldsymbol{r_i}|q)\, dr_1 \ldots dr_q \\ &= \iint_{\boldsymbol{r_i}} 1 - \prod_{i=1}^{q}(1 - \varkappa \frac{1}{1+\frac{\Delta}{\nu}r_i}) f(\boldsymbol{r_i}|q)\, dr_1 \ldots dr_q. \end{aligned} \tag{24}$$

Given that the SBS distances from the VR users are identically and independently distributed, we can rewrite $f(\boldsymbol{r_i}|q) = f(r_1)\ldots f(r_q|q) = (f(r|q))^q$, thus:

$$P(\Lambda|q) = \int_{r=0}^{r=\Omega}\left[1 - \prod_{i=1}^{q}(1 - \varkappa \frac{1}{1+\frac{\Delta}{\nu}r_i})\right]\prod_{i=1}^{q}(\frac{2r_i}{\Omega^2})dr$$

$$= \prod_{i=1}^{q}\left[\left(\int_{r=0}^{r=\Omega}\frac{2r}{\Omega^2}dr\right) - \left(\int_{r=0}^{r=\Omega}\frac{2r}{\Omega^2}(1 - \varkappa \frac{1}{1+\frac{\Delta}{\nu}r})dr\right)\right],$$

$$= \left(\int_{r=0}^{r=\Omega}\frac{2r}{\Omega^2}dr\right)^q - \left(\int_{r=0}^{r=\Omega}\frac{2r}{\Omega^2}(1 - \varkappa \frac{1}{1+\frac{\Delta}{\nu}r})dr\right)^q.$$

This article has been accepted for publication in a future issue of this journal, but has not been fully edited. Content may change prior to final publication. Citation information: DOI 10.1109/JIOT.2022.3142674, IEEE Internet of Things Journal

The second term on the right hand side (without taking it to the power q) can be computed as:

$$A = \int_{r=0}^{r=\Omega} \frac{2r}{\Omega^2}(1 - \varkappa \frac{1}{1+\frac{\Delta}{\nu}r})dr = \frac{2\left(\frac{\nu^2\varkappa\ln(|\Delta\Omega+\nu|)}{\Delta^2} + \frac{\Omega^2}{2} - \frac{\nu\varkappa\Omega}{\Delta} - \frac{\nu^2\ln(|\nu|)\varkappa}{\Delta^2}\right)}{\Omega^2}.$$

Simplifying further we get,

$$A = \frac{2\left(\nu^2\varkappa\ln\left(|\Delta\Omega+\nu|\right) - \nu^2\ln\left(|\nu|\right)\varkappa\right)}{\Delta^2\Omega^2} - \frac{2\nu\varkappa}{\Delta\Omega} + 1.$$

Consequently, $P(\Lambda|q) = 1 - (1+\varkappa\aleph)^q$, where:

$$\aleph = \frac{2\left(\nu^2\ln\left(|\Delta\Omega+\nu|\right) - \nu^2\ln\left(|\nu|\right)\right)}{\Delta^2\Omega^2} - \frac{2\nu}{\Delta\Omega}. \tag{25}$$

Finally to find the marginal probability of LoS $P(\Lambda)$:

$$P(\Lambda) = \sum_{q=0}^{\infty} P(\Lambda|q)P_Q(q) = \sum_{q=0}^{\infty}\left[(1-(1+\varkappa\aleph)^q)\frac{(\eta_P\pi\Omega^2)^q}{q!}e^{-(\eta_P\pi\Omega^2)}\right] = 1 - \exp\left(\varkappa\aleph\eta_P\pi\Omega^2\right).$$

■

B. Proof of Theorem 1

Proof: Based on (4), we express the transmission delay in terms of the VR content size L, C_L, and α, as follows:

$$\alpha = \frac{L}{P(\Lambda)C_L}, \tag{26}$$

$$\mathbb{E}[\alpha] = \frac{E(L)}{E(P(\Lambda)C_L)}\left\{1 - \frac{\mathrm{Cov}(L, P(\Lambda)C_L)}{E(L)E(P(\Lambda)C_L)} + \frac{\vartheta(P(\Lambda)C_L)}{[E(P(\Lambda)C_L)]^2}\right\}, \tag{27}$$

where the ϑ operator is the variance and Cov is the covariance.

Since the VR image size is constant, and that $P(\Lambda)$ and C_L are independent, we have: $\mathbb{E}[\alpha] = \frac{L}{\mathbb{E}[P(\Lambda)]\mathbb{E}[C_L]}$. Thus, we can now compute the expected value of $P(\Lambda)$ and C_L respectively

$$\mathbb{E}[P(\Lambda)] = \int_0^{2\pi}\left(1 - \exp\left((1-\frac{\omega}{2\pi})Z\pi\right)\right)\frac{1}{2\pi}d\omega \tag{28}$$

$$= 1 - \left(\frac{e^{\pi Z}-1}{\pi Z}\right), \tag{29}$$

where $Z = \varkappa\aleph\eta_P\Omega^2$. Based on (4), the $P(\Lambda)$ acts as a discount factor for the LoS rate. The LoS rate expression has only one random term in (26) which is the interference that follows a normal distribution. Subsequently, the rate is a convex function with respect to interference, and, hence, using Jensen's inequality $C_L(\mu_I) \leq \mathbb{E}[C_L(I)]$. As a result, given that the transmission delay is a concave function of the interference, the previous inequality sign is reciprocated. Consequently,

$$\mathbb{E}[\alpha] \leq \frac{L}{\left(1-\left(\frac{e^{\pi Z}-1}{\pi Z}\right)\right)\left(W\log_2\left(1+\frac{p_0A_0r_0^{-2}e^{-K(f)r_0}}{N_0+\mu_I}\right)\right)}. \tag{30}$$

Next, we need to find the variance of the transmission delay. Given that L is constant, and that $P(\Lambda)$ and C_L are independent, according to the first-order Taylor approximation:

$$\vartheta\left[\frac{L}{P(\Lambda)C_L}\right] \approx \frac{E\left[L\right]^2}{E\left[P(\Lambda)C_L\right]^4}\vartheta\left[P(\Lambda)C_L\right], \tag{31}$$

$$\vartheta(P(\Lambda)C_L) = \mathbb{E}[P(\Lambda)^2]\mathbb{E}[C_L^2] - \mathrm{E}^2[P(\Lambda)]\mathrm{E}^2[C_L].$$

We now compute the second moments of $P(\Lambda)$ and C_L:

$$\mathbb{E}[P(\Lambda)^2] = \int_0^{2\pi}\left(1-\exp\left((1-\frac{\omega}{2\pi})Z\pi\right)^2\right)\frac{1}{2\pi}d\omega \tag{32}$$

$$= 1 + \frac{e^{2\pi Z} - 4e^{\pi Z} + 3}{2\pi Z}. \tag{33}$$

Similarly to the first moment, the rate squared as a function of interference is convex; using Jensen's inequality $C_L^2(\mu_I) \leq \mathbb{E}[C_L^2(I)]$. Consequently, the transmission delay squared is a concave function of the interference, this reciprocates the previous inequality. Hence,

$$\vartheta(P(\Lambda)C_L) \approx \vartheta(P(\Lambda)) = \left[1 + \frac{e^{2\pi Z} - 4e^{\pi Z} + 3}{2\pi Z}\right] - \left[1 - \left(\frac{e^{\pi Z}-1}{\pi Z}\right)\right]^2 = \frac{e^{2\pi Z}(\pi Z - 21) + 4e^{\pi Z} - (2+\pi Z)}{2(\pi Z)^2}. \tag{34}$$

Subsequently, elaborating on (32) and (34):

$$\vartheta\left[\frac{L}{P(\Lambda)C_L}\right] \leq \frac{e^{2\pi Z}(\pi Z-21)+4e^{\pi Z}-(2+\pi Z)}{2(\pi Z)^2}\times \frac{L^2}{\left[\left(1-\left(\frac{e^{\pi Z}-1}{\pi Z}\right)\right)\left(W\log_2\left(1+\frac{p_0A_0r_0^{-2}e^{-K(f)r_0}}{N_0+\mu_I}\right)\right)\right]^4} \approx \frac{L^2}{\left(W\log_2\left(1+\frac{p_0A_0r_0^{-2}e^{-K(f)r_0}}{N_0+\mu_I}\right)\right)^4}V_a(Z). \tag{35}$$

Moreover,

$$C_\alpha^2 = \frac{\vartheta(\alpha)}{E^2[\alpha]} = \frac{1}{\left[\left(1-\left(\frac{e^{\pi Z}-1}{\pi Z}\right)\right)\left(W\log_2\left(1+\frac{p_0A_0r_0^{-2}e^{-K(f)r_0}}{N_0+\mu_I}\right)\right)\right]^2} \times \frac{e^{2\pi Z}(\pi Z-2)+4e^{\pi Z}-(2+\pi Z)}{2(\pi Z)^2}, = \frac{1}{\left(W\log_2\left(1+\frac{p_0A_0r_0^{-2}e^{-K(f)r_0}}{N_0+\mu_I}\right)\right)^2}V_a(Z), \tag{36}$$

where

$$V_a(z) = \frac{e^{2\pi Z}(\pi Z-21)+4e^{\pi Z}-(2+\pi Z)}{2(\pi Z)^2}\frac{1}{\left(1-\frac{e^{\pi Z}-1}{\pi Z}\right)^2}. \tag{37}$$

This article has been accepted for publication in a future issue of this journal, but has not been fully edited. Content may change prior to final publication. Citation information: DOI 10.1109/JIOT.2022.3142674, IEEE Internet of Things Journal

Hence, the mean of the E2E delay can be computed as follows:

$$\mathbb{E}[T_1+T_2]=\frac{1}{\mu_1-\lambda_1}+\left[\left(\frac{\rho_2}{2(1-\rho_2)}\left(C_\alpha^2+1\right)\right)+1\right]\mathbb{E}[\alpha], \tag{38}$$

$$=\frac{1}{\mu_1-\lambda_1}+\mathbb{E}[\alpha]\left[1+\left(\frac{\rho_2}{2(1-\rho_2)}\times\right.\right. \tag{39}$$
$$\left.\left.\left(\frac{1}{\left(W\log_2\left(1+\frac{p_0A_0r_0^{-2}e^{-K(f)r_0}}{N_0+\mu_I}\right)\right)^2}V_a(Z)+1\right)\right)\right],$$

where

$$\mathbb{E}[\alpha]\approx\frac{L}{\left(1-\left(\frac{e^{\pi Z}-1}{\pi Z}\right)\right)\left(W\log_2\left(1+\frac{p_0A_0r_0^{-2}e^{-K(f)r_0}}{N_0+\mu_I}\right)\right)}. \tag{40}$$

■

C. Proof of Lemma 1

Proof: To find the second moment of the E2E delay, we can first derive the second moment of the total waiting time of Q_1 as such, given that it is an M/M/1 queue: $\mathbb{E}[T_1^2]=\frac{2}{(\mu_1-\lambda_1)^2}$. Moreover, to find the second moment of Q_2, we first need to express the Laplace-Stieltjes transform of the total waiting time. This transform is given by [58]:

$$F^*_{T_2}(s)=\frac{(1-\rho_2)F^*_\alpha(s)}{1-\rho_2\left(\frac{1-F^*_\alpha(s)}{s\mathbb{E}[\alpha]}\right)}, \tag{41}$$

Subsequently, using the Laplace-Stieltjes transform properties, we need to compute $\mathbb{E}[T_2^2]=\left.\frac{\partial^2F^*_{T_2}(s)}{\partial s^2}\right|_{s=0}$. Hereafter, finding the higher order derivatives of this expression is challenging given that the limits of the fraction will yield an undetermined result. In order to alleviate this issue, we separate the numerator and the denominator, and compute the limits on their higher order derivatives after applying L'Hôpital's rule. Finally, the numerator and denominator are coherently combined to yield the desired result. Thus,

$$F^*_{T_2}(s)=\frac{A(s)}{B(s)}=\frac{(1-\rho_2)F^*_\alpha(s)}{1-\rho_2\frac{1-F^*_\alpha(s)}{s\mathbb{E}[\alpha]}}, \tag{42}$$

$$\left(F^*_{T_2}(s)\right)''=\frac{(A'B-B'A)'B^2-2BB'(A'B-B'A)}{B^4}, \tag{43}$$

$$\lim_{s\to0}A(s)=(1-\rho_2),\qquad\lim_{s\to0}\frac{d}{ds}A(s)=-(1-\rho_2)\mathbb{E}[\alpha],$$
$$\lim_{s\to0}\frac{d^2}{ds^2}A(s)=(1-\rho_2)\mathbb{E}[\alpha^2].$$

By applying L'Hôpital's rule on the second term of B(s):

$$\lim_{s\to0}B(s)=(1-\rho_2)\lim_{s\to0}\left[\frac{\mathbb{E}[\alpha]}{\mathbb{E}[\alpha]}\right]=(1-\rho_2).$$

By applying L'Hôpital's rule twice on $\frac{d}{ds}B(s)$ and three times on $\frac{d^2B(s)}{ds^2}$:

$$\lim_{s\to0}\frac{d}{ds}B(s)=-\rho_2\frac{\mathbb{E}[\alpha^2]}{2\mathbb{E}[\alpha]},\qquad\lim_{s\to0}\frac{d^2}{ds^2}B(s)=-\frac{\rho_2\mathbb{E}[\alpha^3]}{3},$$
$$\mathbb{E}[\alpha^2]\approx\frac{L^2}{\left[1+\frac{e^{2\pi Z}-4e^{\pi Z}+3}{2\pi Z}\right]\left(W\log_2\left(1+\frac{p_0A_0r_0^{-2}e^{-K(f)r_0}}{N_0+\mu_I}\right)\right)^2},$$
$$\mathbb{E}[\alpha^3]\approx\frac{L^3 6\pi z}{(2e^{3\pi z}-9e^{2\pi z}+18e^{\pi z}-6\pi z-11)}\times$$
$$\frac{1}{\left(W\log_2\left(1+\frac{p_0A_0r_0^{-2}e^{-K(f)r_0}}{N_0+\mu_I}\right)\right)^3}. \tag{44}$$

Finally, we replace all the derivatives in (43), thus obtaining after mathematical manipulation:

$$\mathbb{E}[T_2^2]=\left((F^*_{\bar{s}}(s)\right)''$$
$$=\mathbb{E}[\alpha^2]+\frac{\rho_2\mathbb{E}[\alpha^3]}{3(1-\rho_2)}+\frac{\rho_2\mathbb{E}[\alpha^2]}{2(1-\rho_2)}+\left[\left(\frac{\rho_2}{2(1-\rho_2)}\right)\left(\frac{\mathbb{E}[\alpha^2]}{\mathbb{E}[\alpha]}\right)\right]^2 \tag{45}$$

Hence, we substitute the second moment of the second queue in the expression of the E2E delay. According to Burke's Theorem, Q_1 and Q_2 are independent thus their corresponding waiting times are also independent. The E2E delay is thus given by:

$$\mathbb{E}[(T_1+T_2)^2]=\mathbb{E}[T_1^2]+\mathbb{E}[T_2^2]+2\mathbb{E}[T_1]\mathbb{E}[T_2]$$
$$=\frac{2}{(\mu_1-\lambda_1)^2}+\left(\frac{2}{\mu_1-\lambda_1}\right)\mathbb{E}[\alpha]\left[1+\left(\frac{\rho_2}{2(1-\rho_2)}\times\right.\right.$$
$$\left.\left.\left(\frac{1}{\left(W\log_2\left(1+\frac{p_0A_0r_0^{-2}e^{-K(f)r_0}}{N_0+\mu_I}\right)\right)^2}V_a(Z)+1\right)\right)\right]$$
$$+\mathbb{E}[\alpha^2]+\frac{\rho_2\mathbb{E}[\alpha^3]}{3(1-\rho_2)}+\frac{\rho_2\mathbb{E}[\alpha^2]}{2(1-\rho_2)}+\left[\left(\frac{\rho_2}{2(1-\rho_2)}\right)\left(\frac{\mathbb{E}[\alpha^2]}{\mathbb{E}[\alpha]}\right)\right]^2 \tag{46}$$

■

D. Proof of Theorem 2

Proof: Given that the support of the delay is positive, the support of the GEV needs to be positive as well, thus $\xi_E>0$. Consequently, we can find the first moment of the GEV:

$$\mathbb{E}[(T_1+T_2)_n]=\mu_E+\sigma_E\frac{\Gamma(1-\xi_E)-1}{\xi_E} \tag{47}$$

Comparing (13) and (47), we can recognize by identification the following parameters of the tail of the E2E delay:

$$\frac{\xi_E}{\Gamma(1-\xi_E)-1}=\frac{(2n-1)^{1/2}}{(n-1)}, \tag{48}$$
$$\mu_E=\mathbb{E}[T_e],$$
$$\sigma_E=(\vartheta(T_e))^{\frac{1}{2}}=\left(\mathbb{E}[(T_1+T_2)^2]-\mathbb{E}[T_1+T_2]^2\right)^{\frac{1}{2}}. \tag{49}$$

where n is the number of samples of collected E2E delays, and $T_e=T_1+T_2$ is the E2E delay. After some mathematical

manipulations to the moments obtained in Theorem 1 and Lemma 1, we obtain:

$$\mu_E = \frac{1}{\mu_1 - \lambda_1} + \mathbb{E}[\alpha]\left[1 + \left(\frac{\rho_2}{2(1-\rho_2)} \times \left(\frac{1}{\left(W\log_2\left(1 + \frac{p_0 A_0 r_0^{-2} e^{-K(f)r_0}}{N_0 + \mu_I}\right)\right)^2} V_a(Z) + 1\right)\right)\right], \tag{50}$$

$$\sigma_E^2 = \frac{1}{\mu_1 - \lambda_1} + \mathbb{E}[\alpha^2] + \frac{\rho_2 \mathbb{E}[\alpha^3]}{3(1-\rho_2)} + \frac{\rho_2 \mathbb{E}[\alpha^2]}{2(1-\rho_2)} + \left[\left(\frac{\rho_2}{2(1-\rho_2)}\right)\left(\frac{\mathbb{E}[\alpha^2]}{\mathbb{E}[\alpha]}\right)\right]^2 - \left(\mathbb{E}[\alpha]\left[1 + \left(\frac{\rho_2}{2(1-\rho_2)} \times \left(\frac{1}{\left(W\log_2\left(1 + \frac{p_0 A_0 r_0^{-2} e^{-K(f)r_0}}{N_0 + \mu_I}\right)\right)^2} V_a(Z) + 1\right)\right)\right]\right)^2, \tag{51}$$

$$\frac{\xi_E}{\Gamma(1-\xi_E) - 1} = \frac{(2n-1)^{1/2}}{(n-1)}. \tag{52}$$

■

E. Proof of Lemma 2

Proof: Based on (4), we express the rate in terms of L and α as:

$$C = \frac{L}{\alpha} = W\log_2\left(1 + \frac{p_0 A_0 r_0^{-2} e^{-K(f)r_0}}{N_0 + \sum_{i=1}^{M} p A_o r_i^{-2}}\right), \tag{53}$$

We can see that the only random term in (53) is the interference that is assumed to follow a normal distribution. Subsequently, we can express the interference in terms of the transmission delay α as follows:$\sum_{i=1}^{M} p A_o r_i^{-2} = \frac{N_0\left(1 - 2^{\frac{L}{W\alpha}}\right) + p_0^{\mathrm{RX}}}{2^{\frac{L}{W\alpha}} - 1}$. By applying the transform for PDFs $g(y) = g(x)\frac{\partial x}{\partial y}$ we can find the PDF of transmission delay by transforming the PDF of interference accordingly. We let Υ represent the interference and ζ its derivative with respect to the transmission delay. Then, we have:

$$\Upsilon = \sum_{i=1}^{M} p_i A_o r_i^{-2}, \tag{54}$$

$$\zeta = \frac{d\Upsilon}{d\alpha} \tag{55}$$

$$= \frac{\ln(2)\ln \cdot 2^{\frac{L}{W\alpha}}}{W\alpha^2\left(2^{\frac{L}{W\alpha}} - 1\right)} + \frac{\ln(2)\, L\left(N_0\left(1 - 2^{\frac{L}{W\alpha}}\right) + p_0^{\mathrm{RX}}\right) \cdot 2^{\frac{L}{W\alpha}}}{W\alpha^2\left(2^{\frac{L}{W\alpha}} - 1\right)^2} \tag{56}$$

$$= \frac{\ln(2)\, L p_0^{\mathrm{RX}} \cdot 2^{\frac{L}{W\alpha}}}{W\alpha^2\left(2^{\frac{L}{W\alpha}} - 1\right)^2}. \tag{57}$$

Hence, the transmission delay PDF will be: $\psi_T(\alpha) = g(\Upsilon)\frac{d\Upsilon}{d\alpha} = \zeta g(\Upsilon) = \frac{\zeta}{\sqrt{2\pi}\sigma_I} \exp\left(-\frac{(\Upsilon - \mu_I)^2}{2\sigma_I^2}\right)$.

■

REFERENCES

[1] W. Saad, M. Bennis, and M. Chen, "A vision of 6G wireless systems: Applications, trends, technologies, and open research problems," *IEEE Network*, vol. 34, no. 3, pp. 134–142, May. 2020.

[2] F. Hu, Y. Deng, W. Saad, M. Bennis, and A. H. Aghvami, "Cellular-connected wireless virtual reality: Requirements, challenges, and solutions," *IEEE Communications Magazine*, vol. 58, no. 5, pp. 105–111, Jun. 2020.

[3] E. Bastug, M. Bennis, M. Médard, and M. Debbah, "Toward interconnected virtual reality: Opportunities, challenges, and enablers," *IEEE Communications Magazine*, vol. 55, no. 6, pp. 110–117, Jun. 2017.

[4] G. Pocovi, B. Soret, K. I. Pedersen, and P. Mogensen, "MAC layer enhancements for ultra-reliable low-latency communications in cellular networks," in *Proc. of the IEEE International Conference on Communications Workshops (ICC Workshops)*, Paris, France, May. 2017.

[5] "Service requirements for the 5G system," *3rd Generation Partnership Project (3GPP), TS 22.261 v16.0.0, 06 2017*, 2017.

[6] A. Moldovan, P. Karunakaran, I. F. Akyildiz, and W. H. Gerstacker, "Coverage and achievable rate analysis for indoor terahertz wireless networks," in *Proc. IEEE International Conference on Communications (ICC)*, Paris, France, Jul. 2017, pp. 1–7.

[7] H. Elayan, O. Amin, B. Shihada, R. M. Shubair, and M.-S. Alouini, "Terahertz band: The last piece of rf spectrum puzzle for communication systems," *IEEE Open Journal of the Communications Society*, vol. 1, pp. 1–32, Nov. 2019.

[8] M. S. Shur, "Terahertz plasmonic technology," *IEEE Sensors Journal*, vol. 21, no. 11, pp. 12 752–12 763, Sep. 2020.

[9] N. Pareek, N. Sarkar, and A. Bera, "Exploiting hyperbolic metamaterial as a substrate for graphene surface plasmonic cherenkov thz radiation source," *Applied Physics A*, vol. 126, no. 11, pp. 1–8, Oct. 2020.

[10] S. Li, Y. Xie, J. Meng, W. Du, and J. Zhou, "Ultracompact and dynamically tunable plasmonic thz switch based on graphene microcavity metamaterial," *Optical Review*, vol. 27, no. 3, pp. 271–276, Mar.

[11] P. Scarfe and A. Glennerster, "The science behind virtual reality displays," *Annual Review of Vision Science*, vol. 5, no. 1, pp. 529–547, Jul. 2019.

[12] Ericsson Consumer Lab, Ericsson. 10 Hot consumer trends 2030: The Internet of senses. Stockholm, Sweden. [Online]. Available: https://www.ericsson.com/4ae13b/assets/local/reports-papers/consumerlab/reports/2019/10hctreport2030.pdf

[13] G. Teniou, "3GPP achievements on VR & ongoing developments on XR over 5G." 3GPP/VRIF/AIS 2nd Workshop on VR Ecosystems and Standards,"Immersive Media meets, 2019.

[14] X. Yang, Z. Chen, K. Li, Y. Sun, N. Liu, W. Xie, and Y. Zhao, "Communication-constrained mobile edge computing systems for wireless virtual reality: Scheduling and tradeoff," *IEEE Access*, vol. 6, pp. 16 665–16 677, Mar. 2018.

[15] M. Chen, W. Saad, and C. Yin, "Virtual reality over wireless networks: Quality-of-service model and learning-based resource management," *IEEE Transactions on Communications*, vol. 66, no. 11, pp. 5621–5635, Jun. 2018.

[16] Y. Sun, Z. Chen, M. Tao, and H. Liu, "Communications, caching, and computing for mobile virtual reality: Modeling and tradeoff," *IEEE Transactions on Communications*, vol. 67, no. 11, pp. 7573–7586, Jun. 2019.

[17] J. Park and M. Bennis, "URLLC-eMBB slicing to support VR multimodal perceptions over wireless cellular systems," in *Proc. IEEE Global Communications Conference (GLOBECOM)*, Abu Dhabi, UAE, Dec. 2018.

[18] M. Elbamby, C. Perfecto, M. Bennis, and K. Doppler, "Edge computing meets millimeter-wave enabled VR: Paving the way to cutting the cord," in *Proc. IEEE Wireless Communications and Networking Conference (WCNC)*, Barcelona, Spain, Apr. 2018.

[19] P. Popovski, Č. Stefanović, J. J. Nielsen, E. De Carvalho, M. Angjelichinoski, K. F. Trillingsgaard, and A.-S. Bana, "Wireless access in ultra-reliable low-latency communication (urllc)," *IEEE Transactions on Communications*, vol. 67, no. 8, pp. 5783–5801, Aug. 2019.

[20] M. Angjelichinoski, K. F. Trillingsgaard, and P. Popovski, "A statistical learning approach to ultra-reliable low latency communication," *IEEE Transactions on Communications*, vol. 67, no. 7, pp. 5153–5166, Jul. 2019.

[21] S. Nie, J. M. Jornet, and I. F. Akyildiz, "Intelligent environments based on ultra-massive MIMO platforms for wireless communication in millimeter wave and terahertz bands," in *Proc. of International Conference on Acoustics, Speech and Signal Processing (ICASSP)*, Brighton, United Kingdom, May. 2019, pp. 7849–7853.

[22] H. Sarieddeen, M.-S. Alouini, and T. Y. Al-Naffouri, "Terahertz-band ultra-massive spatial modulation MIMO," *IEEE Journal on Selected Areas in Communications*, vol. 37, no. 9, pp. 2040–2052, Jul. 2019.

[23] J. Du, F. R. Yu, G. Lu, J. Wang, J. Jiang, and X. Chu, "MEC-assisted immersive VR video streaming over terahertz wireless networks: A deep reinforcement learning approach," *IEEE Internet of Things Journal*, Jun. 2020.

[24] A. S. Cacciapuoti, K. Sankhe, M. Caleffi, and K. R. Chowdhury, "Beyond 5G: Thz-based medium access protocol for mobile heterogeneous networks," *IEEE Communications Magazine*, vol. 56, no. 6, pp. 110–115, Jun. 2018.

[25] N. Hassan, M. T. Hossan, and H. Tabassum, "User association in coexisting RF and terahertz networks in 6G," in *Proc. of IEEE Canadian Conference on Electrical and Computer Engineering (CCECE)*, London, Canada, Sep. 2020, pp. 1–5.

[26] C. Chaccour, R. Amer, B. Zhou, and W. Saad, "On the reliability of wireless virtual reality at terahertz (THz) frequencies," in *Proc. of the 10th IFIP International Conference on New Technologies, Mobility and Security (NTMS)*, Canary Islands, Spain, June. 2019.

[27] A. J. McNeil, "Extreme value theory for risk managers," *Departement Mathematik ETH Zentrum*, vol. 12, no. 5, pp. 217–237, 1999.

[28] J. Pender, "Risk measures and their application to staffing nonstationary service systems," *European Journal of Operational Research*, vol. 254, no. 1, pp. 113–126, Oct. 2016.

[29] C. Chaccour, M. N. Soorki, W. Saad, M. Bennis, and P. Popovski, "Risk-based optimization of virtual reality over terahertz reconfigurable intelligent surfaces," in *Proc. of IEEE International Conference on Communications (ICC)*, Dublin, Ireland, June. 2020.

[30] M. Haenggi, *Stochastic geometry for wireless networks*. Cambridge University Press, 2012.

[31] V. Petrov, D. Moltchanov, and Y. Koucheryavy, "Interference and SINR in dense terahertz networks," in *Proc. IEEE 82nd Vehicular Technology Conference (VTC2015-Fall)*, Boston, MA, USA, Sep. 2015, pp. 1–5.

[32] G. Stratidakis, A.-A. A. Boulogeorgos, and A. Alexiou, "A cooperative localization-aided tracking algorithm for THz wireless systems," in *Proc. of IEEE Wireless Communications and Networking Conference (WCNC)*, Marrakesh, Morocco, Apr. 2019, pp. 1–7.

[33] S. A. Hoseini, M. Ding, and M. Hassan, "Massive MIMO performance comparison of beamforming and multiplexing in the terahertz band," in *Proc. IEEE Globecom Workshops (GC Wkshps)*, Singapore, Dec. 2017, pp. 1–6.

[34] O. Erturk and T. Yilmaz, "A hexagonal grid based human blockage model for the 5G low terahertz band communications," in *Proc. of IEEE 5G World Forum (5GWF)*, Silicon Valley, CA, USA, Jul. 2018, pp. 395–398.

[35] M. D. Soltani, A. A. Purwita, Z. Zeng, H. Haas, and M. Safari, "Modeling the random orientation of mobile devices: Measurement, analysis and lifi use case," *IEEE Transactions on Communications*, vol. 67, no. 3, pp. 2157–2172, Nov. 2018.

[36] I. K. Jain, R. Kumar, and S. S. Panwar, "The impact of mobile blockers on millimeter wave cellular systems," *IEEE Journal on Selected Areas in Communications*, vol. 37, no. 4, pp. 854–868, Feb. 2019.

[37] M. Gapeyenko, A. Samuylov, M. Gerasimenko, D. Moltchanov, S. Singh, M. R. Akdeniz, E. Aryafar, N. Himayat, S. Andreev, and Y. Koucheryavy, "On the temporal effects of mobile blockers in urban millimeter-wave cellular scenarios," *IEEE Transactions on Vehicular Technology*, vol. 66, no. 11, pp. 10 124–10 138, Sep. 2017.

[38] J. Kokkoniemi, J. Lehtomäki, and M. Juntti, "A line-of-sight channel model for the 100-450 gigahertz frequency band," *arXiv preprint arXiv:2002.04918*, 2020.

[39] Y. L. Babikov, I. Gordon, S. Mikhailenko, L. Rothman, and S. Tashkun, "HITRAN on the web–a new tool for hitran spectroscopic data manipulation," in *Proceedings of the 12th International HITRAN Conference*, Aug. 2012, pp. 29–31.

[40] R. Zhang, K. Yang, Q. H. Abbasi, K. A. Qaraqe, and A. Alomainy, "Analytical modelling of the effect of noise on the terahertz in-vivo communication channel for body-centric nano-networks," *Nano Communication networks*, vol. 15, pp. 59–68, Mar. 2018.

[41] S. Tarboush, H. Sarieddeen, M.-S. Alouini, and T. Y. Al-Naffouri, "Single-versus multi-carrier terahertz-band communications: A comparative study," *arXiv preprint arXiv:2111.07398*, 2021.

[42] W. Chen, X. Ma, Z. Li, and N. Kuang, "Sum-rate maximization for intelligent reflecting surface based terahertz communication systems," in *Proc. of IEEE/CIC International Conference on Communications Workshops in China (ICCC Workshops)*. Changchun, China: IEEE, Aug. 2019, pp. 153–157.

[43] Y. Wu, J. Kokkoniemi, C. Han, and M. Juntti, "Interference and coverage analysis for terahertz networks with indoor blockage effects and line-of-sight access point association," *IEEE Transactions on Wireless Communications*, Nov. 2020.

[44] A. V. Pechinkin, "On convergence of random sums of random variables to the normal law," *Theory of Probability and its Applications*, vol. 18, no. 2, pp. 380–382, Dec. 1973.

[45] Y. Leng, C.-C. Chen, Q. Sun, J. Huang, and Y. Zhu, "Energy-efficient video processing for virtual reality," in *Proceedings of the 46th International Symposium on Computer Architecture*, Phoenix Arizona, USA, Jun. 2019, pp. 91–103.

[46] K. Zhang, Y. Lyu, and L. Zhang, "Mobile edge computing and resource scheduling of internet of vehicles," in *Proc. of 39th IEEE Chinese Control Conference (CCC)*, Shenyang, China, Jul. 2020, pp. 4290–4295.

[47] D. Gross, J. F. Shortle, J. Thompson, and C. M.Harris, *Fundamentals of Queuing Theory*. Hoboken, New Jersey, USA: John Wiley & Sons, Inc., 1974.

[48] M. Bennis, M. Debbah, and H. V. Poor, "Ultrareliable and low-latency wireless communication: Tail, risk, and scale," *Proceedings of the IEEE*, vol. 106, no. 10, pp. 1834–1853, Sep. 2018.

[49] R. A. Fisher and L. H. C. Tippett, "Limiting forms of the frequency distribution of the largest or smallest member of a sample," in *Mathematical Proceedings of the Cambridge Philosophical Society*, vol. 24, no. 2. Cambridge University Press, Aug. 1928, pp. 180–190.

[50] M. H. Loukil, H. Sarieddeen, M.-S. Alouini, and T. Y. Al-Naffouri, "Terahertz-band mimo systems: Adaptive transmission and blind parameter estimation," *IEEE Communications Letters*, Oct. 2020.

[51] H. A. David and H. N. Nagaraja, "Order statistics," *Encyclopedia of Statistical Sciences*, 2004.

[52] P. Artzner, F. Delbaen, J.-M. Eber, and D. Heath, "Coherent measures of risk," *Mathematical finance*, vol. 9, no. 3, pp. 203–228, Dec. 2001.

[53] GEFORCE® RTX 2080 Ti. [Online]. Available: https://www.nvidia.com/en-us/geforce/graphics-cards/rtx-2080-ti/

[54] GPU Database: NVIDIA GeForce RTX 3080. [Online]. Available: https://www.techpowerup.com/gpu-specs/geforce-rtx-3080.c3621

[55] G. Stratidakis, G. D. Ntouni, A.-A. A. Boulogeorgos, D. Kritharidis, and A. Alexiou, "A low-overhead hierarchical beam-tracking algorithm for thz wireless systems," in *Proc. of IEEE 2020 European Conference on Networks and Communications (EuCNC)*, Dubrovnik, Croatia, Jun. 2020, pp. 74–78.

[56] C. Chaccour, M. N. Soorki, W. Saad, M. Bennis, P. Popovski, and M. Debbah, "Seven defining features of terahertz (THz) wireless systems: A fellowship of communication and sensing," *arXiv preprint arXiv:2102.07668*, 2021.

[57] Ericsson Technology Review, Ericsson. XR and 5G: Extended reality at scale with time-critical communication. Stockholm, Sweden. [Online]. Available: https://www.ericsson.com/en/reports-and-papers/ericsson-technology-review/articles/xr-and-5g-extended-reality-at-scale-with-time-critical-communication?utm_source=LinkedIn&utm_medium=social_organic&utm_campaign=dotcom_social_sharing

[58] J. N. Daigle, *Queueing theory with applications to packet telecommunication*. Springer Science & Business Media, 2005.